DEVELOPMENT OF VARIABLE SLOPE PIECEWISE-BASED BROWN SYMBOLS FOR APPLICATION TO NONLINEAR AMBIGUITY SUPPRESSION

THESIS

John Kurian, Captain, USAF

AFIT/GE/ENG/03-12

DEPARTMENT OF THE AIR FORCE
AIR UNIVERSITY

AIR FORCE INSTITUTE OF TECHNOLOGY

Wright-Patterson Air Force Base, Ohio

The views expressed in this thesis are those of the author and do not reflect the official policy or position of the United States Air Force, Department of Defense, or United States Government.

AFIT/GE/ENG/03-12

DEVELOPMENT OF VARIABLE SLOPE PIECEWISE -BASED BROWN SYMBOLS FOR APPLICATION TO NONLINEAR AMBIGUITY SUPPRESSION

THESIS

Presented to the Faculty

Department of Electrical and Computer Engineering

Graduate School of Engineering and Management

Air Force Institute of Technology

Air University

Air Education and Training Command

In Partial Fulfillment of the Requirements for the

Degree of Master of Science in Electrical Engineering

John Kurian, B.S.E.E

Captain, USAF

March 2003

AFIT/GE/ENG/03-12

DEVELOPMENT OF VARIABLE SLOPE PIECEWISE -BASED BROWN SYMBOLS FOR APPLICATION TO NONLINEAR AMBIGUITY SUPPRESSION

John Kurian, BSEE
Captain, USAF

Approved:

Dr Michael A. Temple (Chairman)	14 Mar 03 Date
Maj Roger L. Claypoole, Jr., Ph.D. (Member)	14 MAR 03 Date
Capt Todd B. Hale, Ph.D. (Member)	14 MAR 03 Date

*Acknowledgement*s

I am deeply grateful to the United States Air Force for giving me the opportunity to engage in a postgraduate program. My sincerest thanks to my research advisor, Dr Michael Temple, who labored with me during the past year. I would also like to thank Major Claypoole and Captain Hale for your guidance and support.

I would never have attempted or finished this program without the support and love of my wife and daughter. Finally, I thank God for being my refuge and my fortress during this academic journey.

John Kurian

Table of Contents

Page

List of Figures

Page

Page

Page

ABSTRACT

In 1962, Palermo used two conjugate Linear Frequency Modulated (LFM) pulses to demonstrate a Non-linear Ambiguity Suppression (NLAS) technique to reduce ambiguous energy in radar returns. Using conjugate LFM pulse coding does not readily extend to larger symbol families and thus is severely limited for *M*-channel ($M > 2$) NLAS applications. Larger families of optimal mutually dispersive codes with higher time bandwidth products are needed to achieve the desired *M*-fold range ambiguity reduction.

Using correlation function rms time duration as an optimization metric, the recently proposed Brown's theorem formulates a deterministic process for designing optimal mutually dispersive symbol sets of arbitrary size. The rms time duration performance of digitized "Brown" symbols is invariant to choice of basis (phase-rate) functions used in the design process, yet improvement in cross-correlation sidelobe performance is directly linked to basis function design. This insight provided the impetus for designing and synthesizing a new set of mutually dispersive symbols based on Variable Slope (VS) piecewise basis functions. The resultant VS piecewise-based "Brown" symbols are used with NLAS processing to demonstrate *M*-fold ambiguity suppression capability. Despite the presence of two undesired ambiguous signal responses having +24.0 dB more signal power relative to the weaker desired unambiguous signal, the NLAS processor effectively suppressed the ambiguous responses. The desired signal peak NLAS output response was approximately 11.0 dB above the noise floor and undesired ambiguous responses were suppressed an average of 10.0 to 12.0 dB – a net improvement of approximately 21.0 to 22.0 dB

DEVELOPMENT OF VARIABLE SLOPE PIECEWISE-BASED BROWN SYMBOLS FOR APPLICATION TO NONLINEAR AMBIGUITY SUPPRESSION

CHAPTER 1. INTRODUCTION

1.1 *Background*

In a simplistic sense, a RAdio Detection And Ranging (radar) system is designed to illuminate an area of interest with electromagnetic energy and process the back-scattered energy to determine the presence (detection) and characteristics (parametric estimation) of objects in the environment. In the earliest stages of development, the radar system was categorized as either a continuous wave (CW) or a pulsed system [1:1]. A CW radar system provides good velocity measurements while pulsed systems offer good range and resolution capability. During World War II, research efforts in the radar arena focused on extending the range detection capability. Although many factors affect radar range detection capability, one solution to enhance performance is increasing the average transmit power (transmitting for a longer time) of the pulsed waveform. However, longer transmit time (pulse duration) corresponds to poorer range resolution; the fundamental design trade-off involves obtaining sufficient average power on the target while preserving waveform range resolution which is inversely related to transmitted pulse duration. As radar development evolved, Woodward noted that "range resolution and accuracy were a function of the signal bandwidth, and not of the transmitted pulse width" [1:2]. Thereafter, radar waveform designers were provided another dimension that could

be used in optimizing radar system performance. A natural consequence of exploiting this dimension was the need for more complex radar receivers capable of detecting the "new" waveforms. With these issues in mind, radar engineers shifted their focus and began investigating various pulse modulation techniques having increased signal bandwidth, and thus desired resolution, while preserving the required average power for detection. Linear Frequency Modulated (LFM) waveforms and receiver designs based on matched filter detection concepts were the first successful outcomes of the new paradigm shift in radar engineering.

1.2 *Radar Range Ambiguity*

In a pulsed radar system, the Pulse Repetition Interval (PRI) controls the time delay between pulse transmissions. The variation of PRI leads to ambiguities in both range and Doppler measurements. As the accuracy of range measurements improve with changes in PRI, Doppler estimation performance degrades. Changes in PRI affect radar range and Doppler parametric estimation in opposite ways. Range ambiguities are mainly caused by a periodic transmission of successive pulses, the responses of which are coherently summed by the receiver during a given coherent processing interval (usually equal to one PRI). In such a situation, the radar receiver inaccurately attributes the current processed response to the most recently transmitted pulse and produces inaccurate range measurements. This research effort focuses on processing techniques, a combination of waveform coding and nonlinear signal processing, to resolving range ambiguous responses in high Pulse Repetition Frequency (PRF) radar systems.

Without affecting Doppler accuracy, one approach to resolve range ambiguities is to uniquely code each transmitted pulse and build a receiver structure to uniquely identify each corresponding pulse return. The detection of coded pulse returns is widespread in digital communications applications. In most cases, Matched Filter detection is employed to discriminate code responses of interest. The signal separation performance of this energy detection scheme is based on having "good" correlation code properties in modulated waveforms. In the context of signal separability, "good" code properties include: a focused (compressed) response when correlating with the code of interest and a flat (dispersed) response when correlating with all other codes. Although digital communication applications share many commonalities with radar, there are some unique characteristics inherent in the nature of radar pulse returns. For example, in terrain mapping radar, ground clutter reflections act as strong interferers and prevent the detection of weaker unambiguous target responses. As a result, the detection processes for radar signals require good code properties and additional radar specific signal processing techniques to discriminate the pulse response of interest.

In 1962, Palermo used two conjugate LFM pulses to demonstrate a Non-Linear Ambiguity Suppression (NLAS) signal processing technique to reduce ambiguous energy in processed radar returns [2]. This technique employed interpulse (pulse-to-pulse) coding to distinguish between radar pulse returns while exploiting the compression and dispersion properties of intrapulse (within the pulse) LFM coding to suppress ambiguous energy levels. The suppression operation consisted of the following processes: compression, non-linear threshold, and dispersion. In the compression process, the energy of an undesired pulse is focused using a filter matched for that code. Compression

effectiveness is related to the focused response mainlobe energy concentration and resolution. The non-linear threshold operation was designed to limit the compressed response at a predetermined energy level. The energy limiting process relied on both compression effectiveness and low sidelobe structure (indicating mutual dispersiveness) of cross-correlation responses to remove only the undesired energy. In the dispersion process, the initial signal (before compression) is reconstructed to its original form *without* contributions of the suppressed undesired signal. Suppression processing continues in an iterative fashion until only the signal of interest remains in the processed radar return. This signal is then match filtered and the target response determined from the processed returns with reduced ambiguous energy levels. Using this NLAS process, Palermo demonstrated a two-fold improvement in unambiguous range.

Achieving an *M*-fold improvement in ambiguity resolution relies on the existence of larger code families possessing LFM-like properties. Most discrete codes do not posses the compression *and* cross-correlation dispersive properties desired for NLAS applications. As a result, Brown formulated a deterministic process for designing optimal mutually dispersive symbols of arbitrary size and achieving the finest resolution [3]. The resultant symbols are optimal in rms time duration of correlation functions, with the dispersive nature determined by the square of the Euclidean distance between weighted linear combinations of optimal basis functions and final resolution a function of the symbol envelope. Although symbols generated using Brown's prescribed process demonstrate optimality in terms of the rms time duration metric, the cross-correlation dispersion characterized by the sidelobe metrics is not optimal for NLAS applications. Thus, phase-rate functions yielding Brown symbols that exhibit optimal dispersion in

terms of both the correlation rms time duration *and* sidelobe metrics must be designed for NLAS applications.

1.3 *Research Goal*

The goal of this research is to:

1. Describe a systematic process for designing new basis functions providing improvement over previously developed Brown symbols. Specifically, consider variable slope piecewise basis functions and characterize resultant Brown symbol performance.
2. Demonstrate the impact associated with designing Brown symbols with a uniform spectral taper and *implementing* with a cosine spectral taper.
3. Characterize the effect that time windowing (truncating) band limited Brown symbols has on NLAS system implementation and performance.
4. Characterize NLAS detection and ambiguity suppression effectiveness using Brown symbols. Detection performance is characterized relative to conventional matched filter performance.

1.4 *Thesis Organization*

Chapter II introduces pulse compression theory and outlines metrics used to characterize Brown symbol performance and NLAS effectiveness. The NLAS concept is explained in light of desirable code properties while the adaptive reserved code threshold technique is introduced as a means to suppress ambiguous energy levels. Finally, the

Brown symbol development is offered as a mechanism for generating codes that are well-suited for NLAS applications.

Chapter III explains a new envelope exchange implementation approach aimed at improving Brown symbol cross-correlation sidelobe performance (dispersion) while preserving waveform rms time duration. An analysis for design trade-off impacts is established and the verification process for a new variable slope piecewise-based Brown symbol design is presented. Generation specifications for band limited Brown symbols are analyzed in light of time windowed implementing of these signals. Finally, the experimental set-up for demonstration NLAS ambiguity suppression using the new Brown symbols NLAS is presented.

Chapter IV presents the results from analysis, design and synthesis of Brown symbols based on the new variable slope piecewise basis function. Parameter characteristics for generating Brown symbols that are least sensitive to time windowing are presented. Lastly, NLAS ambiguity suppression capability is quantified for Brown symbols generated with various basis functions. Brown symbol performance is benchmarked relative to LFM waveform coding while NLAS suppression and detection capability is established relative to conventional matched filtering.

Chapter V provides a summary of the research results and contributions. Efforts to improve ambiguity suppression using NLAS are discussed and recommendations for future research provided.

CHAPTER 2. BACKROUND

2.1 *Origin of Pulse Compression*

The study of pulse compression theory must first address the motivation leading to its development for optimizing radar waveform performance. To this end, most studies begin pulse compression analysis using the fundamental radar range equation, given by [5:7]:

$$R_{max} = \sqrt[4]{\frac{P_t G^2 \lambda^2 \sigma}{(4\pi)^3 S_{min}}} \tag{2-1}$$

where R_{max} is the maximum detection range, P_t is the average transmit power, G is the transmit and receive gain (equal in the monostatic radar case), $\lambda = c/f$ is the transmit wavelength, σ is the target radar cross-section, and S_{min} is the minimum required detectable signal strength. Equation (2-1) shows the relationship between maximum detection range (R_{max}), transmission parameters (P_t, G, λ) and received signal power (G, σ, S_{min}). Variation of parameters in (2-1) provided the initial framework for optimizing radar performance, yet this variation alone did not provide desired results and several issues remained unresolved, including [1]:

a) The inefficient use of available average power to the radar transmitter – limited mainly by range resolution constraints

b) The lack of resolution in both range and velocity (Doppler)

c) The vulnerability of radar signals to interfering signals

d) The shortfalls in parameter estimation

In the quest to improve radar performance, Woodward's contribution led to the development of pulsed radar waveforms having higher average power capability without needing increased peak transmitter power or degrading pulse resolution [1:2]. R.H. Dicke was the first to formalize an efficient transmission approach based on Woodward's idea. He proposed the use of Linear Frequency Modulated (LFM) waveforms with a linear time delay pulse compression filter (Matched Filter) [4:1].

2.2 *LFM Waveform Properties*

By varying the sinusoid frequency, in proportion to the modulating signal amplitude, the spectral content (bandwidth) of the signal increases. This form of frequency modulation (FM) is widely used, versus amplitude modulation (AM), in radar applications to improve transmission efficiency [5:341]. Wideband FM designs offer improved output signal-to-noise ratio (SNR) when compared with AM [6:341]. In pulsed radar systems employing LFM waveforms, the transmitted pulse is designed with a relatively long duration while linearly frequency modulating the carrier. The span of LFM modulation is determined by required resolution while the time duration is set according to the energy required to achieve the desired detection range [7]. This generation process was made possible by Woodward's decoupling of range detection and resolution. The long pulse duration increases available average power at transmission and thereby extends range detection capability. For detecting LFM waveforms, a

receiver having linear time versus frequency delay characteristics is used to compress the received signal in time, effectively increasing the signal's peak power and providing improved range resolution. Figure 2-1 shows the magnitude of the compressed filter output characteristics for an LFM waveform with total frequency span (bandwidth) of *B*.

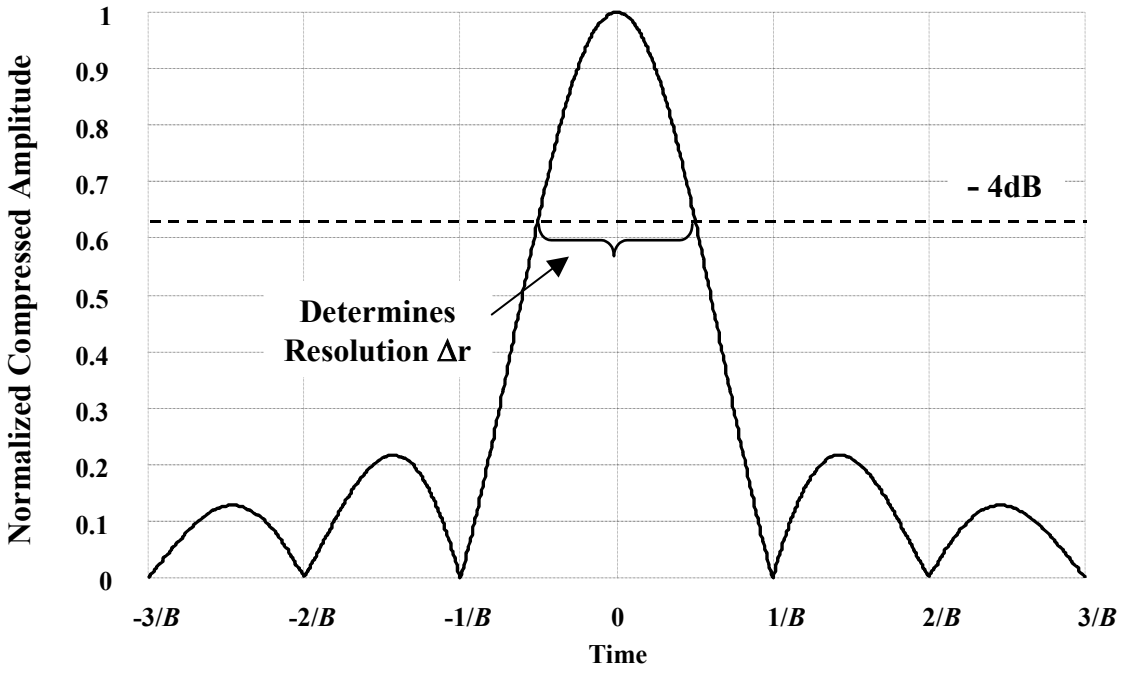

Figure 2-1. Normalized Compressed Output of LFM Waveform Using Linear Time Versus Frequency Delay Filter.

2.2.1 *Resolution.*

Radar resolution is defined as the ability to separate two closely-spaced scatterers [8]. The compressed LFM waveform envelope in Figure 2-1 approximately follows a sinc(t) = sin(t)/t response (under high bandwidth condition) and has resolution Δr defined by:

$$\Delta r = \frac{c}{2B} = \frac{c\tau}{2} \tag{2-2}$$

where c represents the speed-of-light, B is the modulated signal bandwidth and □is the compressed pulse duration measured at – 4.0 dB points relative to the compressed peak response of the time function. As the LFM frequency span (B) increases, the FM modulated signal bandwidth increases and resolution (Δr) improves (decreases). The improvement in resolution is attributed to a decrease in the mainlobe width (time domain) of Figure 2-1 resulting from increased bandwidth. In other words, high bandwidth signals provide more information about the illuminated environment's electromagnetic characteristics and enable better range resolution or distinction of two closely spaced targets.

2.2.2 *Pulse Compression Ratio (PCR) and Time bandwidth (TB) Product.*

The pulse compression ratio (*PCR*) and time bandwidth product (*TB*) for an LFM waveform having an ideal rectangular spectral response is:

$$PCR = \frac{T}{\tau} = TB \tag{2-3}$$

\where T is the transmitted waveform duration, τ is the compressed pulse duration (as previously defined) and B is the transmitted signal bandwidth. As the waveform envelope changes, the relationship in (2-3) becomes an approximate relationship. If the waveform is not modulated (no compression), $B = 1/T$ and $TB = 1$. For a modulated waveform, $B = 1/\tau$ and $\tau < T$ results in $TB > 1$, i.e., systems employing pulse compression have *TB* products greater than one. It is also common to study waveform properties of statistical densities using moments. This type of rigorous waveform characterization is prevalent in the analysis of precision and resolution performance [9].

The "energy function" of a signal can be defined as the modulus squared of the signal representation in the time or frequency domain. The first moment of this energy function, normalized by the signal energy, is used to describe "center of mass" of the energy function in time and frequency respectively as:

$$\begin{aligned} t_c &= \frac{1}{E}\int_{-\infty}^{\infty} t \mid x(t)\mid^2 dt \\ f_c &= \frac{1}{E}\int_{-\infty}^{\infty} f \mid X(f)\mid^2 df \end{aligned} \tag{2-4}$$

The second-order moments of the energy function, specifically the root mean squared (rms) duration, provides a measure of signal energy "spread" in the time (σ) and frequency (Σ) domains as [9:37]:

$$\begin{aligned} \sigma &= \left[\frac{1}{E}\int_{-\infty}^{\infty}(t-t_c)^2 \mid x(t)\mid^2 dt\right]^{\frac{1}{2}} \\ \Sigma &= \left[\frac{1}{E}\int_{-\infty}^{\infty}(f-f_c)^2 \mid X(f)\mid^2 df\right]^{\frac{1}{2}} \end{aligned} \tag{2-5}$$

Introducing the rms duration of signals leads to the notion of "effective" time and "effective" frequency when discussing signal properties. This leads to "effective" time-bandwidth product ($\sigma \cdot \Sigma$) which is bounded by Gabor [10] as:

$$\sigma \cdot \Sigma \geq 1 \tag{2-6}$$

2.2.3 *Compressed Envelope Sidelobe Properties.*

Increasing bandwidth effectively decreases the main lobe width of the compressed LFM pulse response. The envelope sidelobes decrease as a function of time displacement from pulse center and stays constant, relative to the peak response, with increased bandwidth.

If an LFM waveform is generated with a uniform spectrum and filtered with a matched version of itself, the peak sidelobe level (PSL) of (2-7) will never vary from – 13.2 dB [11:537, 12]. In (2-7), compressed filter response $\theta(x,x)$ is generated by correlating a waveform using n time delays and sampling the received responses at a rate such that the response extremes are captured.

$$PSL = 10\log\left[\frac{\max\limits_{n \neq 0} n \left|\theta_n(x,x)\right|^2}{\left|\theta_0(x,x)\right|^2}\right] \tag{2-7}$$

One approach for changing PSL level is to change the pulse's spectral shape. This comes at the cost of lowering signal-to-noise ratio and increasing the first null width of the *sinc(t)* response in Figure 2-1 [13]. Lower sidelobe levels are generally desirable to decrease the false alarm probability in environments with high target density. As a result, waveform design achieving having low PSL levels is an important aspect in determining "optimal" waveform shape.

Similarly, the integrated side-lobe level (ISL) metric of (2-8) provides a measure of total energy distributed in the sidelobes. When pulse compression is used in radar imaging applications, a high concentration of signal strength in the main lobe is needed for target detection and resolution [12]. This requirement dictates the use of waveforms having low ISL levels.

$$ISL = 10\log\left[\frac{\sum_{\substack{m=1-M \\ m\neq 0}}^{M-1}\left|\theta_m(x,x)\right|^2}{\left|\theta_0(x,x)\right|^2}\right] \tag{2-8}$$

Both PSL and ISL can be used to characterize the compression filter response when the transmitted waveform is correctly matched at the receiver. When the compression filter is mismatched to a signal *y*, in place of *x*, the PCCL level defined in (2-9) becomes another important factor in characterizing waveform performance. This metric shows the difference in power between the peak compressed power and the sidelobe levels in a mismatched scenario. A dispersed response with low PCCL levels is characteristic of LFM waveforms.

$$PCCL = 10\log\left[\frac{\max_n\left|\theta_n(x,y)\right|^2}{\max\left\{\left|\theta_0(x,x)\right|^2,\left|\theta_0(y,y)\right|^2\right\}}\right] \tag{2-9}$$

2.3 *Traditional Approaches to Resolve Range Ambiguity*

There are three basic approaches to resolving range ambiguities, including, 1) using multiple PRI's, 2) Frequency Modulation (FM) ranging, and 3) pulse coding [14:1-18]. In the multiple PRI approach, the transmitter sends bursts of pulses at various pulse repetition intervals. The radar receiver processes the pulse returns to determine target range. If a target's range at varying PRI's is not constant, a range ambiguous situation is indicated. This approach relies heavily on selecting the correct set of PRI's

for determining range. Research efforts focused on optimizing PRI selection include the Chinese remainder theorem [5:176], the residual look-up table algorithms [15], the major-minor Pulse Repetition Frequency(PRF) method and the M:N method [16:274-277]. Although all these methods are relatively simple to implement, the major shortfall in using a multiple PRI approach is the inability to coherently process between multiple PRI bursts, thus reducing the overall coherent processing interval [14]. On a positive note, the multiple PRI method mitigates eclipsing loss, i.e., loss of target returns when the transmitter is sending out pulses in a radar system where only a single antenna is employed.

The FM ranging approach utilizes Doppler shift to calculate the actual target range. A timing mark embedded in the transmitted pulse (through a modulation process, such as linear FM) allows the receiver to calculate the time delay [16:289]. Although the radar operator may find the FM ranging approach effective for determining single target range, this approach fails in a target rich environment. As the number of targets increases, the operator is unable to distinguish between closely spaced targets.

The pulse coding approach to range ambiguity resolution relies on the transmission of diversely coded pulses and an effective signal processing architecture for uniquely identifying processed signal returns. This approach to ambiguity resolution using NLAS receiver architecture is described in Section 2.4.

2.4 *Nonlinear Ambiguity Suppression (NLAS) Approach*

For NLAS processing, unique coding is applied to individual pulses (intrapulse coding) on a pulse-by-pulse basis (interpulse coding) such that received ambiguous returns may be attributed to individually transmitted pulses. For M-channel NLAS processing, each channel consists of $M-1$ elemental suppression operations (ESO) followed by matched filtering for the code response of interest [17]. Figure 2-2 is the k^{th}-stage of ESO processing using the adaptive reserved code thresholding (ARCT) technique that will be presented in Section 2.4.2. In the ESO, the ambiguous (undesired) coded u_j response is compressed (focused) by matched filter $h_j[n]$ and coded u_k responses ($k = 1, 2, \ldots, M$ and $k \neq j$) are dispersed (defocused) – the goal is to produce output $y_k[n]$ devoid of u_j responses.

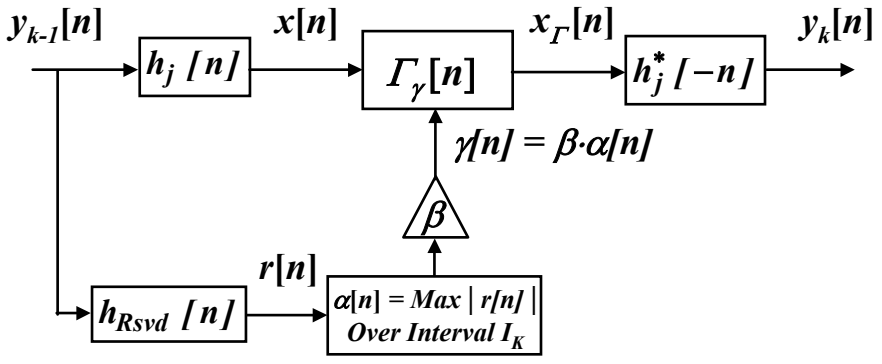

Figure 2-2. k^{th}-Stage Elemental Suppression Operation with Adaptive Reserved Code Thresholding (ARCT)

Suppression is accomplished using a non-linear "hole punch" operation given by (2-10):

$$\Gamma_{\gamma}[n] = \begin{cases} 0 & \mid x[n] \mid > \gamma[n] = \beta \cdot \alpha[n] \\ x[n] & Elsewhere \end{cases} \tag{2-10}$$

Non-linearity $\Gamma_{\gamma}[n]$ suppresses (zeros) all $x[n]$ samples having a magnitude greater than $\gamma[n] = \beta \cdot \alpha[n]$. Suppressed response $x_{\Gamma}[n]$ is then conjugate matched filtered for u_j by $h_j^*[-n]$, ideally yielding output $y_k[n]$ having original u_k ($k \neq j$) responses and residual components of the suppressed u_j response. By applying the ESO $M-1$ times, each NLAS channel operates at an effective PRI of M times the original PRI thereby achieving M times the unambiguous range.

2.4.1 *NLAS Code Selection.*

Using conjugate LFM pulses for diverse pulse coding does not readily extend to larger symbol families and thus is severely limited for M-channel ($M > 2$) NLAS applications. Larger families of optimal mutually dispersive codes with higher time bandwidth products are needed to achieve the desired M-fold range ambiguity reduction. Consistent with Section 2.2.3, the PSL, ISL and PCCL are common metrics for quantifying ideal NLAS code characteristics. Ideal NLS codes must exhibit good *aperiodic* autocorrelation *and* cross correlation performance (low sidelobes levels). Symbol sets comprised of pseudo-random discrete codes, such as Gold codes, exhibit mutual dispersion properties [14] but are not optimum for NLAS. Similarly, codes generated from combinatorial optimization methods, such as simulated annealing (SA), exhibit good dispersion properties yet are constrained by the inability to efficiently generate codes of longer length [14]. Given the inability to find optimal sets of discrete NLS codes, Brown's

optimal mutually dispersive analog code development process will be considered next, as described in Section 2.5. These codes are optimal in terms of the rms duration of the correlation functions and exhibit superior compression and dispersion properties.

2.4.2 *Adaptive Reserved Code Thresholding.*

Adaptive reserved code thresholding (ARCT) exploits code cross-correlation (dispersive) properties to provide maximum suppression of ambiguous clutter while having minimal impact on desired unambiguous responses. In ARCT, one code is *reserved* (not transmitted) and used to adaptively "train" threshold shape ($\alpha[n]$) and scale (β). The $h_{Rsvd}[n]$ of Figure 2-2 is the reserved code matched filter with output $r[n]$ consisting exclusively of dispersed code responses, i.e., no autocorrelation effects are present since the reserved code was not transmitted. ARCT shape $\alpha[n]$ is established as the maximum value of $|r[n]|$ over a pre-defined interval of length K (I_K). The resultant $\alpha[n]$ is scaled by β to produce the final ARCT of $\gamma[n] = \beta \cdot \alpha[n]$.

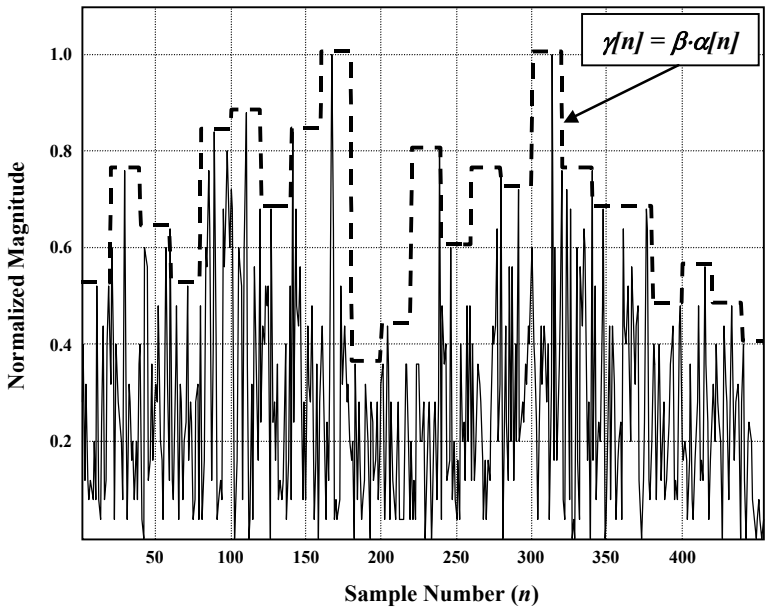

Figure 2-3. ARCT (Dashed Line) Overlaid on Dispersed Filter Response (Solid Line). Results for $M = 3$, 127-Length 16-SA Codes with $\beta = 1$ and $K = 20$.

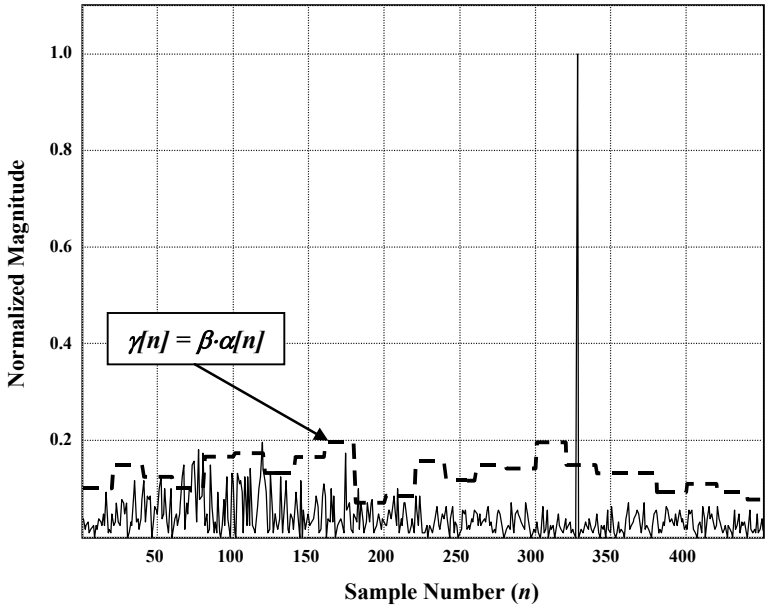

Figure 2-4. ARCT of Figure 2-3 (Dashed Line) Overlaid on Focused Filter Response (Solid Line). Results for $M = 3$, 127-Length 16-SA Codes with $\beta = 1$ and $K = 20$.

Figure 2-3 shows a representative ARCT (dashed line) overlaid on the $h_{Rsvd}[n]$ response (solid line) used to generate it. This $\gamma[n]$ is for three $M = 127$ length 16-SA codes using $K = 20$, $\beta = 1$, and two coded signals centered at sample #101 and #328 to form ambiguous data. In Figure 2-4 this $\gamma[n]$ is overlaid on the $h_j[n]$ response containing one focused (matched) response at sample #328 and one dispersed response centered at sample #101. ARCT $\gamma[n]$ exhibits two desirable features: 1) it falls below the focused response causing maximum undesired energy suppression and 2) it effectively tracks the dispersed response causing minimal desired energy loss.

2.5 *Brown Symbol Design Process*

The following Brown symbol development process parallels [18]. The search for mutually dispersive codes begins by considering a pulse coded radar signal given by:

$$x(t) = \sum_{k=0}^{M-1} f_k\left(t - kT\right) \tag{2-11}$$

where T is the Pulse Repetition Interval (PRI) and $f_k(t)$ has a Fourier transform of the form:

$$F_k(\omega) = \sqrt{A(\omega)}\, e^{\,j\Phi_k(\omega)} \quad A(\omega), \Phi_k(\omega) \in \Re \tag{2-12}$$

The k^{th} Matched Filter processed pulse return is represented as follows:

$$\begin{aligned} F_l(\omega)H_k(\omega) &= F_l(\omega)F_k^*(\omega) \equiv P_{lk}(\omega) \\ &= A(\omega)e^{j[\Phi_l(\omega)-\Phi_k(\omega)]} \end{aligned} \tag{2-13}$$

When $k = l$, the processed output represents a matched filter response whose inverse Fourier transform is the signal autocorrelation function (ACF), $\rho_{kk}(t)$ given by:

$$P_{kk}(\omega) \overset{\Im^{-1}}{\Rightarrow} \rho_{kk}(t) \tag{2-14}$$

The NLAS process requires the ACF to be as compressed as possible and the crosscorrelation function (CCF) (mismatched filter response) to be as dispersed (flat) as possible. The rms time duration of correlation functions, σ_{lk} as defined in (2-15), are used to quantify correlative dispersion [9:37]. This definition of σ_{lk} assumes $\rho_{lk}(t)$ is normalized to unity energy and centered at $t = 0$; the dot operator ($\cdot$) in (2-15) and (2-16) represents differentiation with respect to frequency.

$$\sigma_{lk} \equiv \left[\int_{-\infty}^{\infty} t^2 \left| \rho_{lk}(t) \right|^2 dt \right]^{\frac{1}{2}} = \left[\frac{1}{2\pi} \int_{-\infty}^{\infty} \left| j \dot{P}_{lk}(\omega) \right|^2 d\omega \right]^{\frac{1}{2}} \tag{2-15}$$

$$\sigma_{lk} = \left[\frac{1}{2\pi} \int_{-\infty}^{\infty} \dot{A}^2(\omega)\, d\omega + \frac{1}{2\pi} \int_{-\infty}^{\infty} \left[\dot{\Phi}_l(\omega) - \dot{\Phi}_k(\omega) \right]^2 A^2(\omega) d\omega \right]^{\frac{1}{2}} \tag{2-16}$$

For $k = l$ in (2-16), σ_{kk} represents the ACF rms time duration and is purely a function of envelope $A(\omega)$ (second term of second equation identically cancels). To achieve a maximally compressed ACF response, the first term of (2-16) is made as small as possible; this provides the impetus for designing optimal envelope $A(\omega)$ such that the ACF rms time duration , σ_{kk} is minimized. Similarly, to achieve a large dispersed response, the CCF rms time duration, $k \neq l$ in, (2-16) is made as large as possible; the σ_{lk} dispersion has contributions due to both the envelope and the phase functions. With the

envelope minimization constraint in place, the phase functions are designed to optimize the CCF rms duration.

Optimality in compression and mutual dispersion is achieved using the following process [18]:

1) For optimal compression, the envelope is derived from the solution to the following constrained optimization problem:

$$\begin{aligned} &\textit{Minimize} && \frac{1}{2\pi}\int_{-\infty}^{\infty} \dot{A}^2(\omega)d\omega \\ &\textit{Such that} && \frac{1}{2\pi}\int_{-\infty}^{\infty} A^2(\omega)d\omega \;=\; 1 \end{aligned} \tag{2-17}$$

Using calculus of variations, a cosine envelope of the following form is derived:

$$A(\omega) = \sqrt{\frac{4\pi}{\Omega_0}}\cos\left(\frac{\pi\omega}{\Omega_0}\right) \qquad |\omega| \le \frac{\Omega_0}{2} \tag{2-18}$$

2) For M symbols, use any set of M maximally equidistant unit-vectors in M-dimensional space (hermits), $\boldsymbol{C} = [\boldsymbol{c}_0\ \boldsymbol{c}_1\ \boldsymbol{c}_2\ \ldots\ \boldsymbol{c}_{M\text{-}1}]$. One solution to this hermit problem is defined as follows [18]:

$$\boldsymbol{C} = \frac{1}{\sqrt{M^2 - M}}\begin{bmatrix} M-1 & -1 & -1 & \cdots & -1 \\ -1 & M-1 & -1 & \cdots & -1 \\ -1 & -1 & M-1 & \cdots & -1 \\ \vdots & \vdots & \vdots & \ddots & \vdots \\ -1 & -1 & -1 & \cdots & M-1 \end{bmatrix}_{M\times M} \tag{2-19}$$

3) Choose any set of odd basis functions given by

$$\boldsymbol{\varphi}(\omega) = [\boldsymbol{\varphi}_0(\omega)\ ,\ \boldsymbol{\varphi}_1(\omega)\ ,\ \boldsymbol{\varphi}_2(\omega)\ ,\ \ldots\ ,\ \boldsymbol{\varphi}_{M-1}(\omega)]^{\mathrm{T}} \tag{2-20}$$

while satisfying spectral window orthonormality given by:

$$\frac{1}{2\pi}\int_{-\infty}^{\infty}\boldsymbol{\varphi}_k(\omega)\,\boldsymbol{\varphi}_l(\omega)\,A^2(\omega)\,d\omega = \delta_{kl} \quad \begin{cases} 1\ k = l \\ 0\ \textit{Otherwise} \end{cases} \tag{2-21}$$

4) Describe M phase-rate functions of the form $\dot{\Phi}_k(\omega) = \sqrt{G_D}\,\mathbf{c}_k^T\boldsymbol{\varphi}(\omega)$, where G_D is a dispersive gain factor, (the dot above represents differentiation) yields phase functions of the form:

$$\Phi_k(\omega) = \sqrt{G_D}\ \mathbf{c}_k^T \int_{\omega}\boldsymbol{\varphi}(\omega)\,d\omega \tag{2-22}$$

5) Resultant time and frequency domain expressions for mutually dispersive codes are expressed as:

$$\begin{aligned} f_k(t) &= \frac{1}{2\pi}\int_{-\Omega_0/2}^{\Omega_0/2}\sqrt{A(\omega)}\,e^{\,j\,[\,\omega t + \Phi_k(\omega)\,]}\,d\omega \\ F_k(\omega) &= \sqrt{A(\omega)}\ e^{\,j\,\Phi_k(\omega)} \end{aligned} \tag{2-23}$$

It can be shown that symbols designed using this *process* yield basis independent CCF rms time duration of:

$$\sigma_{kl} = \left[\sigma_{kk}{}^2 + \frac{2M}{M-1}G_D\right]^{\frac{1}{2}} \tag{2-24}$$

If the optimal cosine taper envelope is used, the ACF rms time duration σ_{kk} becomes:

$$\sigma_{kk} = \frac{\pi}{\Omega_o} \tag{2-25}$$

with relatively constant PSL of –23dB and ISL of –18dB at low bandwidth ($\Omega_0 < 5000$ Rad/sec) simulations.. As the cosine taper bandwidth increases, the ACF rms duration decreases, compression improves and ISL levels should theoretically decrease [3].

CHAPTER 3. METHODOLOGY

3.1 *Introduction*

Ambiguity suppression capability of the NLAS processing system hinges on the selection of codes which possess 1) good autocorrelation compression (focusing) with low integrated sidelobe levels and 2) maximum cross-correlation dispersion across all pulse codes within the code family [19]. This chapter describes various stages of the Brown symbol development process, including design, synthesis, and concept demonstration. Section 3.3 outlines the motivation, symbol parameters, performance metrics, and validation techniques used for the Brown symbol design process. Section 3.3 addresses factors involved in transitioning from band limited, infinite time duration signals (as resulting from the Brown symbol design process) to realizable finite duration signals as obtained through temporal windowing. Finally, Section 3.4 outlines the methodology used for demonstrating range ambiguity resolution using Brown symbols with a NLAS system.

3.2 *Brown Symbol Design Process*

The rms time duration of correlation functions is the optimization metric used for Brown symbol design. Although cross-correlation performance of optimal mutually dispersive symbols, in terms of the rms metric, is independent of phase rate (or basis) function form, the symbol dispersive properties indicated by the peak cross-correlation

sidelobe metric is directly linked to phase rate function design. Optimal mutually dispersive symbols for NLAS applications must exhibit good performance in cross-correlation metrics, including high rms time duration *and* low PCCL. Brown symbols generated from different basis functions may achieve equivalent rms time duration yet differ greatly in PCCL performance. This divergence has paved the way for the design of "optimum" phase rate functions yielding minimal PCCL levels.

3.2.1 *Basis Function Constraints.*

Basis function selection is guided by the spectral window orthogonal properties exhibited by the function family. The spectral windowing constraint in (2-21) is determined by the symbol's correlation envelope in the frequency domain to obtain the finest possible resolution (in terms of rms metric) for specified system bandwidth [20]. Although many functions exhibit orthogonal spectral properties, the optimum cosine spectral window constraint in (2-18) "eliminates" them from being good candidates for basis functions. A design trade-off can be made by relaxing the spectral window constraint (loss of resolution) to permit the use of other functions, i.e., Chebyshev, or to allow basis function implementations that are not orthogonal within the optimal cosine taper. The impact of such a trade-off must be analyzed in terms of the resultant cross-correlation rms time duration and sidelobe metrics.

3.2.2 *Validating Symbol Design.*

By using the rms time duration metric, Brown symbol development effectively isolates the envelope $A(\omega)$ and phase-rate function components of the symbol in the spectral

domain as shown in (2-16). If basis functions $\varphi_i(\omega)$ are designed using a "non-optimum" envelope with the *prescribed* design process, the cosine-specific compression expression of (2-25) is no longer valid but the basis invariant dispersion performance of (2-24) is maintained. However, if the "non-optimum" envelope has jump discontinuities and/or the phase functions have discontinuities where the envelope is non-zero, the interchange used to derive (2-16) no longer holds [3]. Similarly, if Brown symbols are generated using basis functions *designed* for a "non-optimum" envelope and *implemented* with the cosine spectral envelope, the optimal compression in (2-25) is achieved but the basis invariant dispersion performance in (2-24) is compromised. Although the basis independent dispersion performance is degraded with the envelope exchange implementation, the dispersive gain parameter G_D can still be used to achieve the needed dispersion, albeit *not equally* affecting the cross-correlation between all the symbols.

3.2.3 *Benchmarking Symbol Performance.*

The time bandwidth (*TB*) product is proposed as a key metric for providing "equivalent" comparison of Brown symbol performance with LFM coded waveforms. As indicated earlier, Brown symbols are windowed in the time domain since band limited signals have infinite duration in time and are unrealizable. As a result, effective symbol time duration (σ_k) is used to guide the time windowing process such that $\geq 99.9\%$ of the total signal energy is retained in time-windowed symbols. This time duration and the intermediate frequency bandwidth of Brown symbols are used to calculate the *TB* metric. Performance of LFM coded waveforms is used as a benchmark since this coding approach provides "near optimal" baseline NLAS performance [14:4-19]. Both LFM and

Brown coded symbols are forms of analog coding (versus discrete) that are capable of achieving high pulse compression ratios. The impact of design trade-offs relative to LFM provides a good baseline for comparing performance of Brown symbols generated with different basis functions.

3.2.4 *Parameters for Improving Cross-Correlation Characteristics.*

The Brown symbol design process clearly shows the impact of increased symbol bandwidth and dispersion on the rms duration of correlation functions in (2-24) and (2-25). Improvement in the rms time duration metrics does not necessarily indicate improved sidelobe characteristics. For example, although Brown symbol ACF compression improves with bandwidth, PSL levels remain relatively constant. The invariant nature of the PSL metric is exhibited in LFM coded waveforms as well. LFM PSLs remains constant at –13.23 dB (corresponding to a rectangular spectral window) with increased bandwidth; LFM waveform PSLs can be reduced by sub-sampling [12]. Given the lack of a mathematical framework for capturing the impact of rms time duration and bandwidth on cross-correlation *sidelobe* metrics, the impact of increasing rms time duration (through dispersive gain) and bandwidth on symbol sidelobe performance is experimentally characterized. The experimental process is constrained here by available computational resources which are quickly exhausted when attempting to simulate high bandwidth scenarios.

Previous research results demonstrated improvements in the PCCL metric as dispersive gain G_D increases across basis functions [18:4-14 to 4-28]. The measure of improvement was directly tied to the "nature" of the basis functions. However, the impact of changing

bandwidth on PCCL was not completely developed nor understood. This impact is characterized relative to basis function selection for symbols designed using the same specifications.

3.3 *Symbol Sensitivity to Time Windowing*

The dispersive gain parameter, G_D, in Brown symbol design process provides the capability to improve cross-correlation rms time duration performance at the cost of spreading the signal in time. Although the impulse-like qualities of the time signals are "flattened" by increasing cross correlation function variance, the associated time to transmit 99.9% of signal energy increases. The effect of time windowing Brown symbols generated with various dispersive gains and bandwidths, and consequently varying TB product, is qualitatively analyzed in light of sideloble degradation. Results from this analysis provide a heuristic approach to generating symbols best suitable for windowing. Given research time constraints, time windowing analysis was only performed for one type of basis (VS piecewise) and $M = 4$ symbols. As summarized in Table 3-1, time windowing was performed with the following specifications of each scenario: 1) dispersive gain G_D value of 0dB (low) with Ω_o (rad/sec) value of 8π (low) and resulting time bandwidth TB value of 7.15 (low), and 2) dispersive gain G_D value of 40dB (high) with Ω_o (rad/sec) value of 8π (low) and resulting time bandwidth TB value of 563 (medium) and 3) dispersive gain G_D value of 40dB (high) with Ω_o (rad/sec) value of 40π (high) and resulting time bandwidth TB value of 1002 (high).

Table 3-1. Experimental Scenarios for Testing Brown Symbol "Sensitivity" to Time Windowing.

	Scenario 1	Scenario 2	Scenario 3
G_D	0	40	40
Ω_0	8π	8π	40π
TB	7.15	563	1002

3.4 *NLAS Performance Using Brown Coded Waveforms*

After developing and characterizing an "acceptable" set of Brown coded waveforms, the ambiguity suppression capability of NLAS processing is demonstrated using the Brown coded waveforms. The experimental scope is limited to demonstration and characterization of range ambiguity suppression capability for point target returns of diversely coded pulses. Many detection techniques can provide for range resolution of point target returns, yet the capabilities are limited when the unambiguous target of interest is embedded in very strong ambiguous (interference) returns. The NLAS range resolution capability in the presence of strong interference is bench marked to the traditional matched filter detection approach.

3.4.1 *System Components and Limitations*

The scenarios considered are not intended to demonstrate clutter suppression capability nor do they take into account the effects of complex, distributed target returns. Fixed signal-to-noise (SNR) ratios and ambiguous signal power levels are also used. The effects of SNR variation are not considered.

3.4.2 *Constraints*

Scenario characteristics that remain constant throughout experimentation are defined as *constraints*. The following *constraints* are maintained constant through all scenarios:

a) Relative Signal-to-Noise Ratio (SNR): The relative input SNR between unambiguous (desired) and ambiguous (undesired) signals is fixed at –24.5 dB for all experiments. The noise power is held constant using a single noise realization for all simulated scenarios.

b) Ambiguous Input Signal Specifications: The number of ambiguous (undesired) input signals is fixed at two with each having +24.5 dB more power than the unambiguous (desired) input signal. An arbitrary phase shift of $\pm 90^0$ is applied to the ambiguous signals to induce signal propagation phase delay effects. Signal powers are adjusted in each ambiguous signal to achieve SNR of 0.0 dB. This condition is maintained throughout all scenarios.

c) Symbol Time Bandwidth (*TB*) Product: Symbol time bandwidth (*TB*) product is maintained at approximately 7100 for all coded waveforms employed in NLAS processing characterizations. Although symbol parameters, other than the hermit weights, may vary independently, *TB* is maintained constant for all the symbols.

d) Time Windowed Symbol Energy: Brown symbols are generated having high *TB* and time windowed (truncated) such that their energy level is greater than 99% of their total energy. A high TB is used to minimize the impacts time windowing (truncation).

e) NLAS Thresholding: An adaptive reserved code threshold (ARCT) is used for all NLAS processing involving Brown Symbols. The only exception occurs when LFM coded waveforms are used due to the limited number of symbols ($M = 2$), since one symbol must be held in reserve for ACRT. In the LFM scenarios, the NLAS processor uses a constant threshold value yielding the lowest threshold is .

3.4.3 *Factors*

Scenario characteristics that change throughout experimentation are defined as *factors*. The following factors were changed during the scenarios:

a) Symbols Used for NLAS Processing: Two types of coded waveforms (symbols) are used for NLAS characterization in various scenarios, including 1) Brown symbols generated with various basis functions and 2) LFM symbols.

b) Signal Detection Techniques: Both conventional matched filtering and NLAS processing are used to detect the unambiguous (desired) signal response.

c) Ambiguous Signal Response Locations: A time delay is induced on each ambiguous (undesired) input signal as a means to vary correlation interference levels. In one case, the time delay is zero for both ambiguous signals such that they *completely overlap* the unambiguous signal in time. In the second case, a time delay of plus and minus one-half the pulse width is induced such that the ambiguous signals *partially overlap* the unambiguous signal in time.

3.4.4 *Experimental Setup for NLAS Demonstration*

For NLAS ambiguity resolution demonstration, four uniquely coded, equal energy Brown symbols were generated. The weaker *unambiguous* input signal $s_U(t)$ was created using symbol $f_0(t)$ and random noise $n(t)$, as shown in (3-1), and *ambiguous* input signal $s_A(t)$ was created by adding two symbols to $s_U(t)$ as shown in (3-2). The remaining symbol $f_3(t)$ was used by the NLAS processor to generate adaptive reserved code thresholds (ARCT) for suppressing ambiguous signal responses.

$$s_U(t) = f_0(t) + n(t) \tag{3-1}$$

$$s_A(t) = s_U(t) + \alpha f_1(t - t_1) + \beta f_2(t - t_2), \qquad \alpha, \beta \in C \qquad t_k \in \Re \tag{3-2}$$

3.4.5 *Performance Metrics and Collection Process*

Data from the metric collection process is used to accurately quantify NLAS ambiguous energy suppression capability relative to matched filter performance. For comparison, the "noise floor" and various peak responses (energy levels) of the matched filter detection of $f_0(t)$, as depicted in Figure 3-1, are determined for the following scenarios:

a) Best Case: Only $s_U(t)$ of (3-1) is present

b) Completely Overlapped Case: $s_A(t)$ of (3-2) is also present with $t_k = 0$

c) Partially Overlapped Case: $s_A(t)$ of (3-2) is also present with $t_1 = -T$ and $t_2 = T$ for T the symbol duration.

Similarly, the "noise floor" and suppressed peak responses (energy levels) for NLAS processing is determined for the following scenarios:

a) Best Case: Only $s_U(t)$ of (3-1) is present and an ARCT is used

b) Coloration Scenario: $s_A(t)$ of (3-2) is also present with $t_k = 0$ (completely overlapped) and an infinite threshold is used. The coloration is primarily introduced by the dispersion operation.

c) Suppressed Scenario: $s_A(t)$ of (3-2) is also present with $t_k = 0$ (completely overlapped) and an ARCT is used

d) Steps (b) and (c) are repeated for the *partially overlapped* scenario with $t_1 = -T$ and $t_2 = T$ for symbol duration T.

Figure 3-1 summarizes the scenarios (for each interference level) for NLAS ambiguity suppression demonstration. The "best case" response, i.e., the best response that can be achieved given no ambiguous signals are present, is used to normalize all other scenarios using the same processing scheme (MF or NLAS) for the following reasons:

a) To characterize the effect of ambiguous signals on detection capability. The ambiguous energy levels introduced in the correlation response must be quantified relative to detection in the no interference case.

b) To quantify ARCT effectiveness in preserving the unambiguous signal.

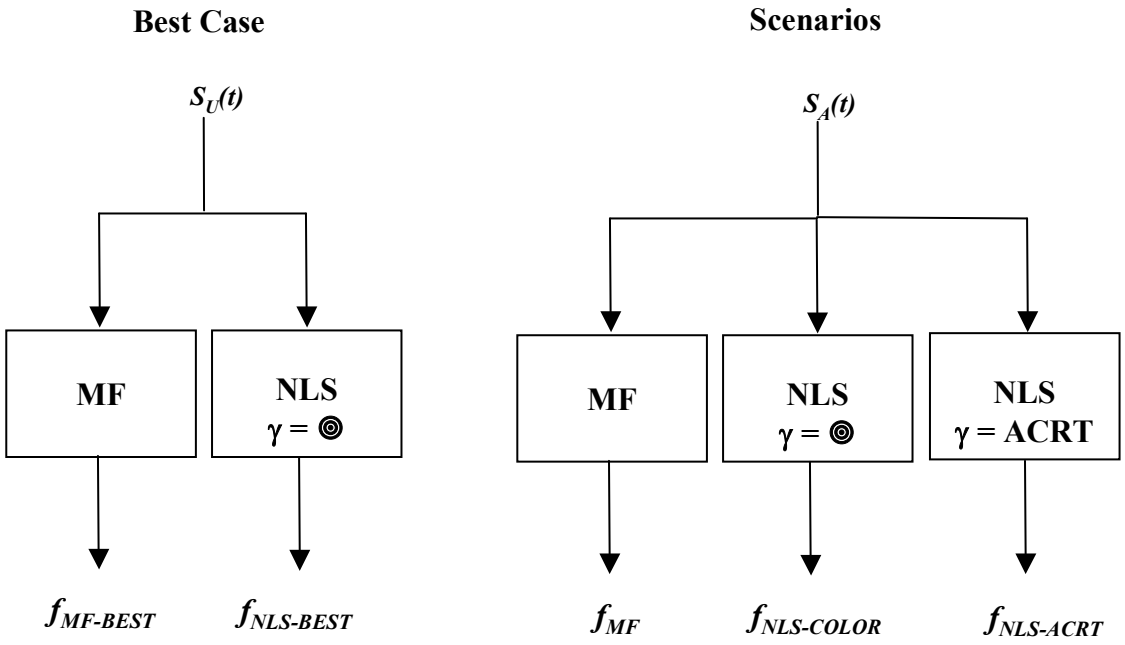

Figure 3-1. Scenarios for NLS Demonstration.

Figure 3-2 depicts how model metrics are collected and used to quantify the NLAS suppression performance, relative to matched filtering.

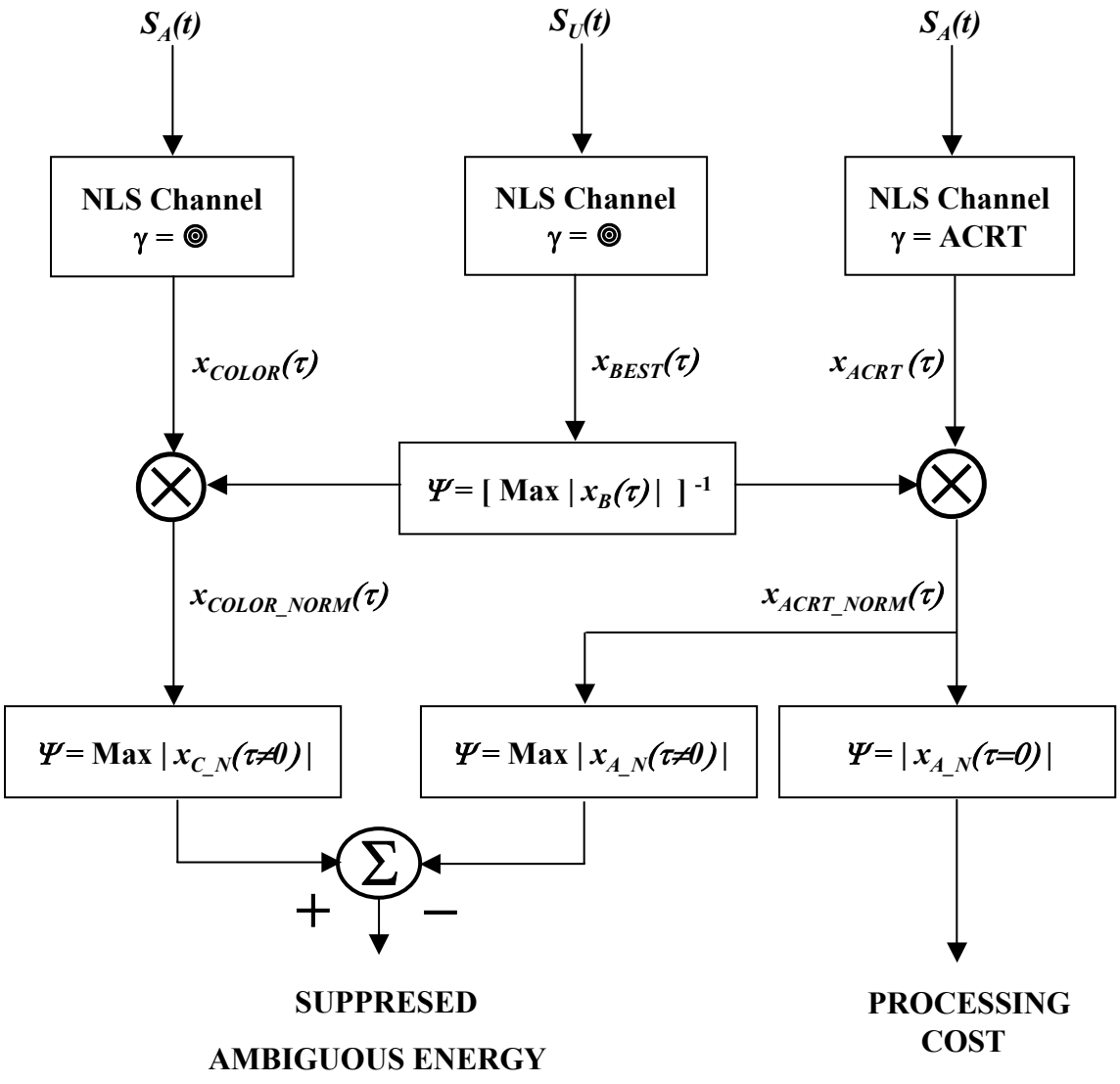

Figure 3-2. Metric collection process for NLS demonstration.

CHAPTER 4. ANALYSIS AND RESULTS

4.1 *Introduction*

The root mean squared (rms) time duration of correlation functions is the corner stone metric of Brown symbol development. Using the rms time duration metric of (2-15), Section 4.2 outlines the process for generating a new family of mutually dispersive Brown symbols that exhibit properties of the LFM chirp waveforms and sinusoidal functions.

4.2 *New Family of Brown Symbols*

To characterize performance of Brown symbols generated with a sinusoidal basis, a pair of LFM symbols having equivalent time bandwidth (*TB*) product is generated. In this comparison, the Brown symbols exhibited equivalent or better performance in all areas except PCCL levels [18]. This shortfall led to the design of a new family of variable slope (VS) piecewise basis (phase rate) functions having LFM-like chirp characteristics while possessing the intrinsic orthogonal property of sinusoids.

4.2.1 *Variable Slope (VS) Piecewise Basis Functions.*

Basis function development begins by considering the following sinusoids within a normalized uniform spectral window: *sin(t), sin(3t), sin(5t),* and *sin(7t)*. The uniform spectral envelope provides for design of orthonormal basis functions satisfying (2-21) using systems of equations – ease of design.. Only the positive half of the spectral

window is considered during the actual development process since the basis functions $\varphi_i(\omega)$ are designed to have odd symmetry. Basis function amplitudes vary between ± 1. The first VS piecewise basis function in the family, $\varphi_0(\omega)$, is the traditional LFM up-chirp as shown in (4-1). Subsequent members are designed to be orthonormal to this function and all other family members. Four family members of the VS piecewise basis may be represented as follows:

$$\varphi_0(\omega) = \omega \qquad 0 < \omega < 1 \tag{4-1}$$

$$\varphi_1(\omega) = \begin{cases} \frac{1}{a}\omega & 0 < \omega < 1 \\ \frac{2}{a-1}\omega - \frac{a+1}{a-1} & a < \omega < 1 \end{cases} \tag{4-2}$$

$$\varphi_2(\omega) = \begin{cases} \frac{1}{b}\omega & 0 < \omega < b \\ \frac{2}{b-c}(\omega - b) + 1 & b < \omega < c, \quad b < a < c \\ \frac{2}{1-c}(\omega - 1) + 1 & c < \omega < 1 \end{cases} \tag{4-3}$$

$$\varphi_3(\omega) = \begin{cases} \frac{1}{d}\omega & 0 < \omega < d \\ \frac{2}{d-e}(\omega - d) + 1 & d < \omega < e, \quad d < b < a < e \\ \frac{2}{f-e}(\omega - f) + 1 & e < \omega < f, \quad e < c < f \\ \frac{2}{f-1}(\omega - f) + 1 & f < \omega < 1 \end{cases} \tag{4-4}$$

The parametric solution in Table 4-1 was generated by simultaneously solving (4-1) through (4-4) such that orthonormality is maintained between basis set members.

Table 4-1. Parametric Solution for Four Orthogonal VS Piecewise Basis Functions

a	0.4142
b	0.2094
c	0.6602
d	0.1849
e	0.4547
f	0.7314

As the width of the uniform spectral window increases, these points are merely scaled by the appropriate maximum bandwidth. After defining basis functions over the positive portion of the spectral domain, the odd symmetry of the functions is used to generate the negative spectral responses, i.e., functions generated using (4-1) through (4-4) with parameters of Table 4-1 are reflected about the origin to yield negative spectral responses. The resultant basis function amplitudes are scaled such that they are normalized to unit energy. As the number of desired symbols increases, the set of basis functions must be redesigned. The linear combination of weighted VS basis functions

must satisfy (4-5) since these functions adhere to Brown's basis specifications of (2-21) with $A(\omega)$ being a uniform spectral envelope. Equation (4-5) is a rearrangement (2-24), where σ_{kl}^2 and σ_{kk}^2 are the variance of the cross-correlation function (CCF) and autocorrelation function (ACF), respectively, G_D is a dispersive gain factor and M is the total number of symbols.

$$\sigma_{kl}^2 - \sigma_{kk}^2 = G_D \frac{2M}{M-1} \tag{4-5}$$

4.2.2 *Design Process Validation & Symbol Characterization*

To validate the Brown symbol design process, the following data was collected using Brown symbols based on the new VS piecewise basis functions. Figure 4-1 shows the phase functions generated from (4-1) through (4-4) using parameters of Table 4-1. The $\Phi_0(\omega)$ phase function is similar to an LFM parabolic phase function, with "distortions" introduced from the linear combination of the basis functions and weighting factors associated with hermits and dispersive gain. The distortions are necessary to make the symbols maximally dispersive within the extended family of symbols. The resultant correlation functions in the time are shown in Figure 4-2. The –13.3 dB sidelobe response of the ACF, $\rho_{00}(t)$, is characteristic of a uniform spectral taper. The CCF plots exhibit the desired "flat" correlation responses with low PCCL levels

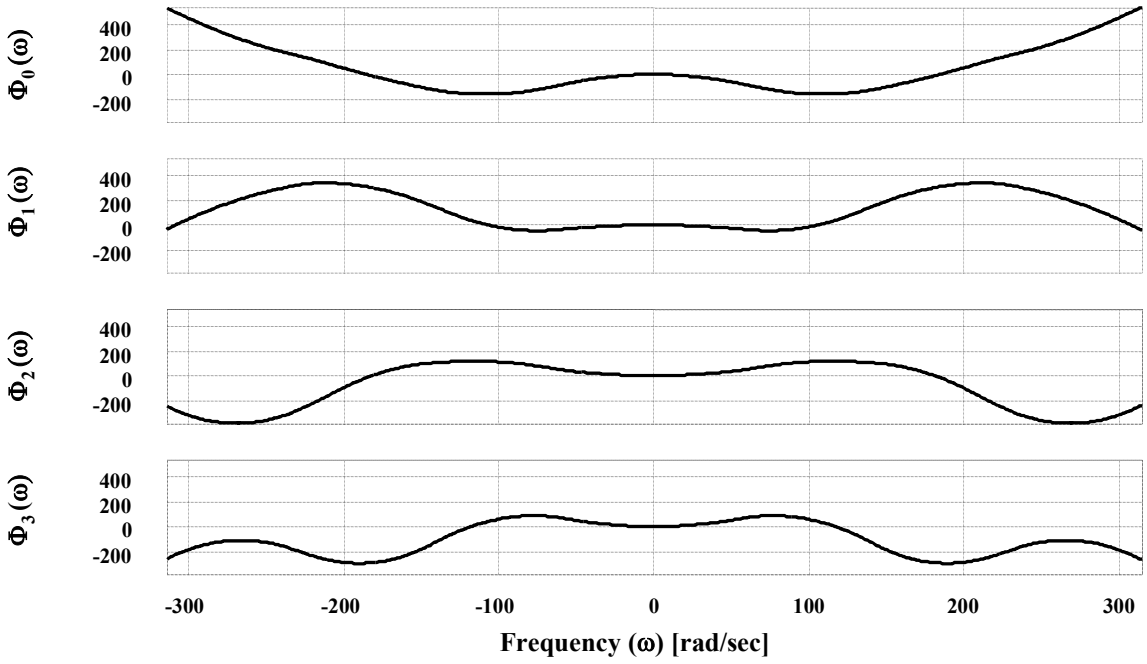

Figure 4-1. Phase Functions for VS Piecewise Basis.

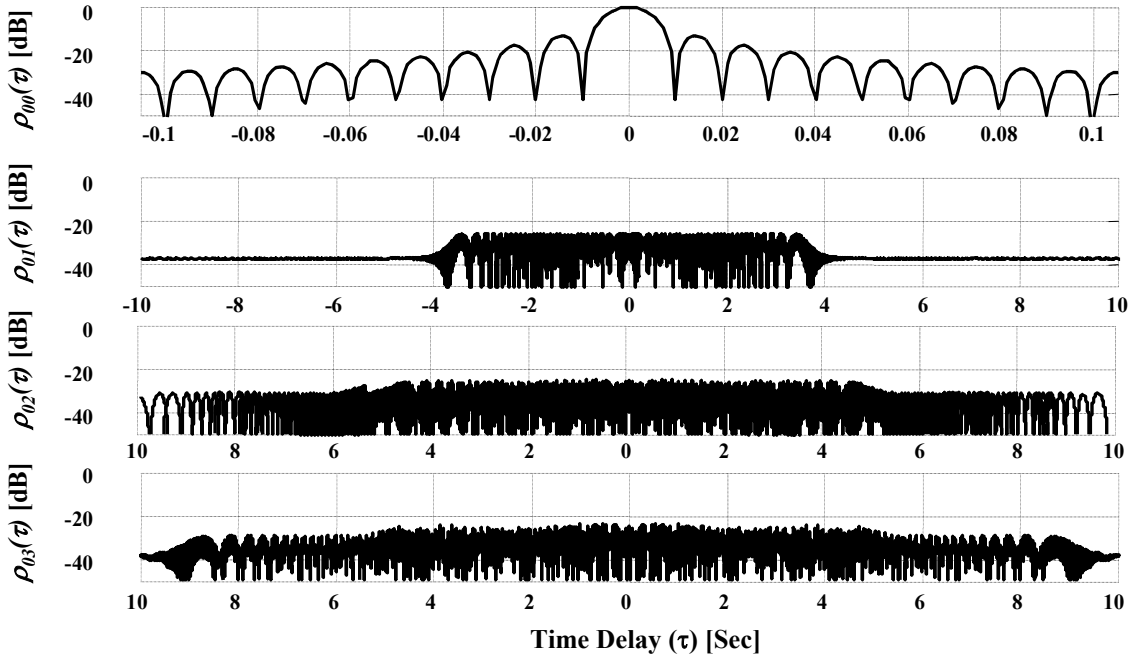

Figure 4-2. Correlation of Brown Symbols Based on VS Piecewise Basis.

Windowed Brown symbols (magnitude shown) containing 99.9% of the original energy are shown in Figure 4-3. The rms time duration of the time signal, σ_k, is used to guide the truncation process; $4.4\sigma_k$ of $f(t)$ was used for these results.

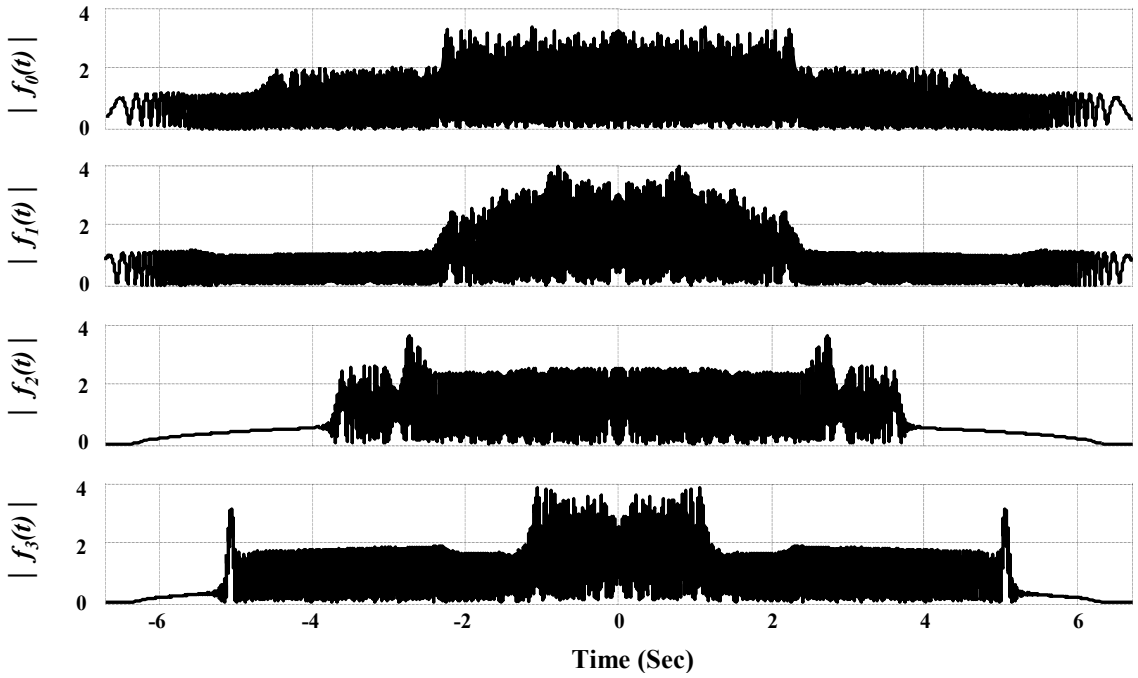

Figure 4-3. Windowed Brown Symbols Containing 99.9% energy

Table 4-2 summarizes the metrics collected from these Brown symbols.

Table 4-2. Brown Symbol Performance: VS Piecewise Basis Functions with Uniform Spectral Taper.

Metrics	
Bandwidth	200π
Dispersive Gain	10
PSL	-13.31 dB
ISL	-7.12 dB
PCCL	-22.5 to –25.9 dB
σ_{kk}^2	16.9×10^{-2} sec
σ_{kl}^2	26.83 sec

Notice that (4-5) is satisfied using the collected metrics for the uniform taper envelope, thus validating the orthonormal basis design accuracy. Unlike the ACF compression expression derived for the cosine taper envelope in (2-25), a closed-form solution of the square taper compression is unlikely to exist. Moreover, the jump discontinuities in the uniform taper envelope endpoints will not allow the interchange in (2-16). The ISL performance of the uniform taper at - 7.12dB is marginal compared to the cosine taper ISL level of –18.84dB. Low ISL, which signifies higher energy concentration in the mainlobe compared to the sidelobes, is critical to effective energy suppression in the NLAS system. Consequently, the VS piecewise basis functions, which were designed to be orthonormal in a uniform taper, is implemented with a cosine taper during the symbol generation process. The performance of symbols generated with the envelope exchange implementation is shown in Table 4-3.

Table 4-3. Brown Symbol Performance: VS Piecewise Basis Functions with Cosine Spectral Taper.

Metrics	
Bandwidth	200π
Dispersive Gain	10
PSL	-23.04 dB
ISL	-18.84 dB
PCCL	-20.5 to –25.0 dB
σ_{kk}^2	2.5×10^{-5} sec
σ_{kl}^2	5.96 to 26.93 sec

Two outcomes result from the envelope exchange implementation, including 1) improved ACF characteristics and 2) degradation of the *equally* mutually dispersive nature as indicated by a CCF rms metric decrease. As expected, the ACF of symbols generated with the cosine taper exhibit superior sidelobe and rms compression performance compared to the rectangular taper. However, the uniform-to-cosine taper exchange

couples the dispersion performance to properties of the basis functions within the implemented envelope; a natural result since VS piecewise basis functions were specifically designed using a uniform taper but implemented with a cosine envelope. As a result, (4-5) no longer governs system performance, i.e., for a given number of symbols M and dispersive gain G_D, the "hermit weights" are no longer the *only* factor affecting cross-correlation rms duration σ_{kl}^2.

4.2.3 *Benchmarking Symbol Performance*

Performance of the "new" VS piecewise-based Brown symbols is benchmarked relative to the performance of LFM symbols having the same time bandwidth (TB) product. A summary of correlation statistics is shown in Figure 4-4.

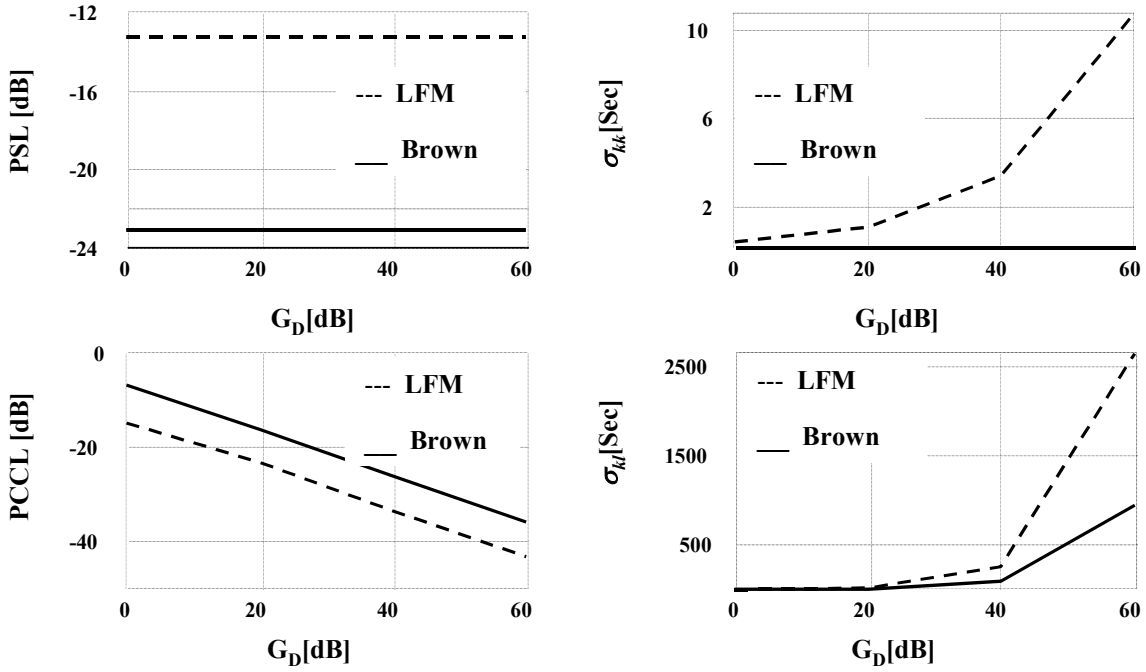

Figure 4-4. Comparison of Correlation Statistics for LFM and VS Piecewise-Based Brown Symbols: M = 2, $\Omega_o = 8\pi$ and Cosine Spectral Taper. (a) PSL, (b)σ_{kk}, (c) PCCL, and (d) σ_{kl}

Results in Figure 4-4 seem to indicate that VS piecewise-based Brown symbols provide better target resolution in a "noiseless" environment. This is characteristic of the lower compression metric σ_{kk} and PSL levels. In terms of PCCL levels, VS piecewise-based Brown symbol performance is poorer by approximately 7.5 dB. However, this performance represents a *4.5 dB improvement* over sinusoidal-based Brown symbols. In other words, sinusoidal-based Brown symbols performed 12.0 dB poorer than LFM at an equivalent TB. As indicated in Figure 4-4, LFM symbols achieve superior performance in terms of σ_{kl}. However, the dispersion for VS piecewise-based Brown symbols is degraded from optimal due to the envelope exchange. If the VS piecewise basis functions had been originally designed using a cosine spectral taper, the dispersion would be equal to that of the LFM symbols. The sinusoidal-based Brown symbols provide performance on par with LFM symbol in terms of σ_{kl} duration.

4.2.4 *Impact of Varying Bandwidth on PCCL levels*

Performance improvement of the chirp-like basis family over the sinusoidal functions is not readily apparent at low bandwidth. While holding the dispersive gain at G_D =1, as symbol bandwidth increases for both basis, σ_{kk} improves, σ_{kl} degrades slightly and PSL and ISL remain constant. However, the PCCL metric changes differently for each basis as shown in Figure 4-5. For the VS piecewise basis, the lower PCCL with increasing bandwidth provides insight into the "flatness" of *f(t)* in the time domain. For the sinusoidal basis, the higher constant PCCL level with increasing bandwidth signifies "impulse like" concentrated energy levels in *f(t)*. At low dispersive gains, the sinusoidal

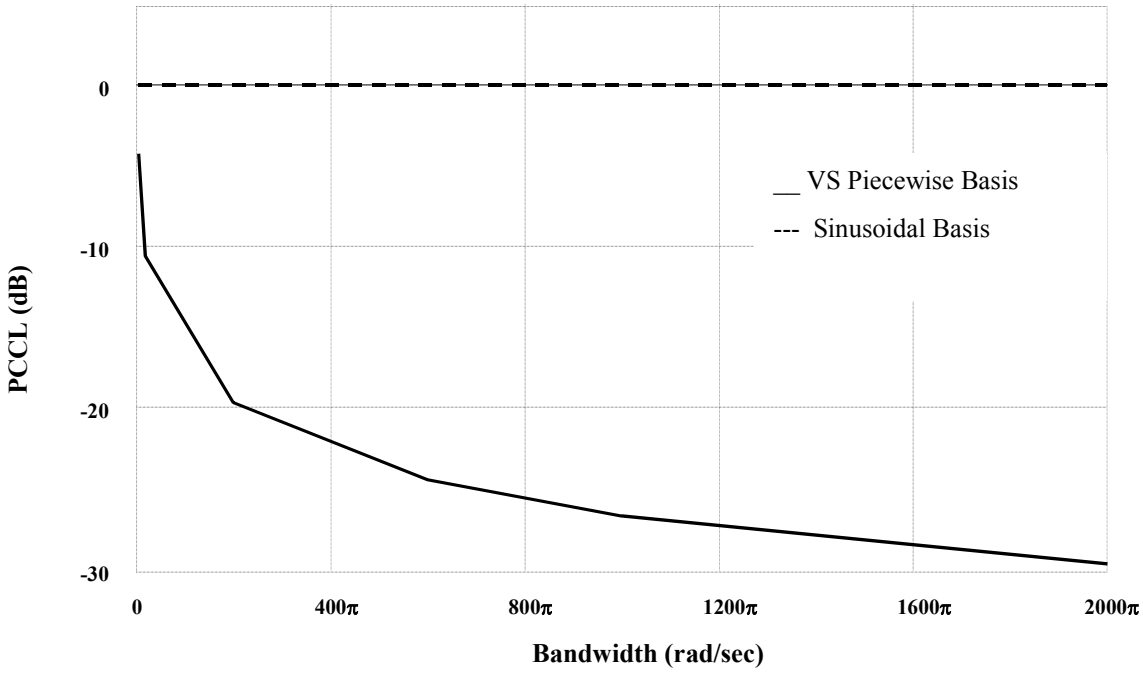

Figure 4-5. Effect of Changing Bandwidth on PCCL Metric with $G_D = 1$.

basis functions tend to generate time signals having impulse like properties. Yet, this effect is not accurately captured in the rms time duration of correlation functions. The design of chirp-like basis functions provides an added parameter (bandwidth) for controlling PCCL levels. The performance improvement gained by increasing bandwidth comes without an increase in required transmit time to capture 99.9% of the symbol energy. Although an increase in dispersive gain G_D also improves PCCL levels, it further increases the equivalent time duration of the signal. Improvements resulting from varying the bandwidth are achieved at the cost of slightly degrading the mutually dispersive symbol properties; increasing G_D can enhance the dispersive symbol nature.

4.2.5 *Comparison of VS Piecewise Basis with CS Piecewise Basis*

VS piecewise basis performance is compared to constant slope (CS) piecewise basis of the following form [18:4-24]:

$$\varphi_n(\omega) = \frac{4a_n\sqrt{3}}{\Omega_0}\left[(\omega + \Omega_0/2)\, rect\left(\frac{\omega + \Omega_0/2 - \Omega_n/8}{\Omega_n/4}\right)\right.$$
$$+ \sum_{m=0}^{2a_n-1}(-1)^m(\omega + \omega_m)\, rect\left(\frac{\omega - \omega_m}{\Omega_n/2}\right) \qquad (4\text{-}6)$$
$$\left. + (\omega - \Omega_0/2)\, rect\left(\frac{\omega - \Omega_0/2 + \Omega_n/8}{\Omega_n/4}\right)\right]$$

where $\Omega_k = \Omega_0 / a_k$, and $\omega_n = \frac{\Omega_0}{2}\left(n/a_k - 1\right)$. The variable a_k is the number of cycles over the intermediate frequency bandwidth Ω_0, Ω_k is the period and ω_n are zero crossings of the basis functions. Once again, this basis functions set was designed using a uniform spectral envelope but is implemented with a cosine spectral taper. Representative CS piecewise basis performance, relative to LFM, is shown in Figure 4-6. A comparison of Figure 4-4 VS piecewise results with Figure 4-6 CS piecewise results reveals relatively equivalent performance when using LFM as the benchmark. However, the dispersive nature of CCF rms duration, σ_{kl}, for the VS piecewise based symbols is marginally superior to the CS piecewise based symbols. This is a testament of the coupling effect between basis function selection and the dispersion exhibited in the envelope exchange implementation. As in the VS piecewise basis case, the CS piecewise basis also provides lower PCCL with increasing bandwidth.

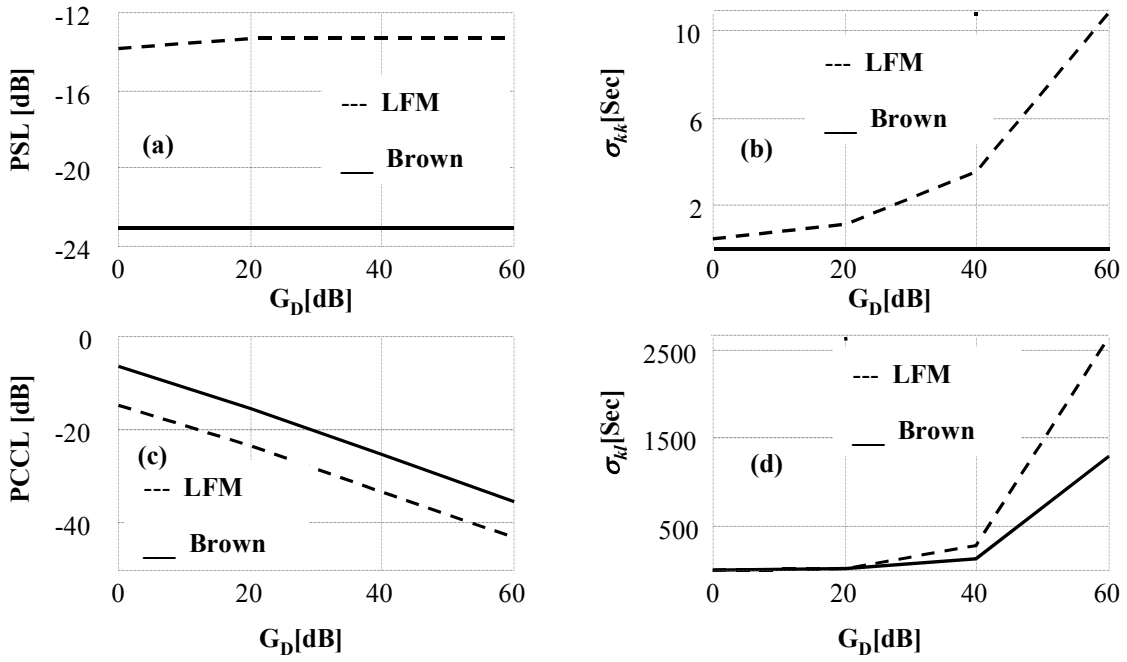

Figure 4-6. Comparison of Correlation Statistics for LFM and CS Piecewise-Based Brown Symbols: M = 2, $\Omega_o = 4\pi$ and Cosine Spectral Taper.
(a) PSL, (b) σ_{kk}, (c) PCCL, and (d) σ_{kl}

4.3 *Symbol Sensitivity to Time Windowing*

The rms time duration (σ_k) of Brown symbols is the key metric that guides the windowing process. This metric provides a measure "spread" in time domain signal *f(t)*, whereas σ_{kl} characterizes the spread of the correlation functions. Although the correlation function rms duration (σ_{kl}) is designed to be equal across the choice of basis functions, the σ_k is not equal. The resultant Brown Symbols are centered at $t = 0$ and normalized by the symbol energy before the windowing (truncation) process is applied. Relative window size for truncation varies with the number of symbols generated, dispersive gain, bandwidth and the basis function choice for generating the Brown Symbols. For generating $M = 2$ symbols with the sinusoidal piecewise basis functions at

$\Omega_0 = 8\pi$, a window duration of at least $6\sigma_k$ of the time function is needed to capture 99.9% of the energy [18] at various dispersive gains. For the VS piecewise based Brown symbols, the relative window size is shown in Figure 4-7 for the same specifications. The effect of increasing the frequency extent to $\Omega_0 = 40\pi$ while keeping all the other parameters constant is also shown on the Figure 4-7. If bandwidth is held constant and dispersive gain G_D increased, the window size needed to capture 99.9% of the energy, in terms of $\sigma_{k,}$ decreases. Although increasing G_D increases the signal time duration, the impulse-like qualities of the signal are flattened out and the signal is more suitable for windowing. When bandwidth is increased in the same scenario, the signal time duration shortens and amplitude increases. Yet, the dispersive gain counteracts this effect and improves the relative "compactness" of the signal in comparison to symbols generated at lower bandwidths. Symbols generated with large dispersive gains and large bandwidths are ideal candidates for time windowing."

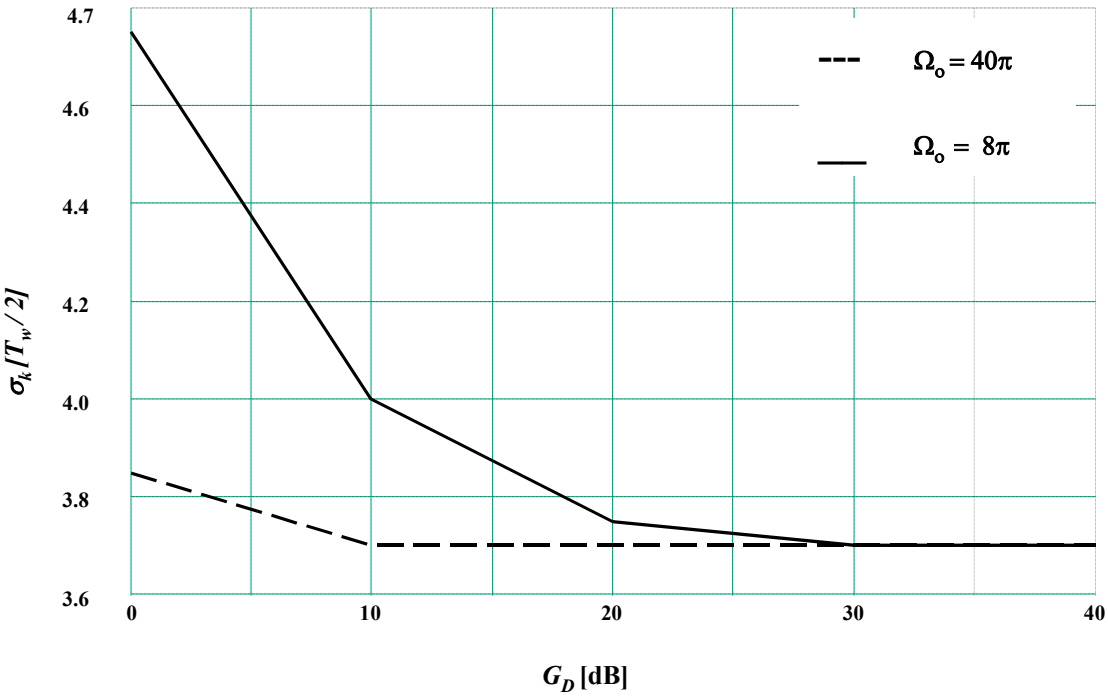

Figure 4-7. VS Piecewise-Based Brown Symbols: Duration Needed to Capture 99.9% of Total Energy.

As dispersive gain G_D increases, the time associated with a window capturing 99.9% of the total energy increases. This increased time duration may pose a problem in applications requiring shorter transmit times. In such a situation, one needs to understand the impact of time windowing symbols below the 99.9% energy level. The impact of time windowing is characterized in terms of signal spectral response and sidelobe metrics of the truncated symbol. Figure 4-8 shows the impact of truncating the energy below the 99.9% level to 86.5% using the following parameters: $\Omega_0 = 8\pi$, $G_D = 1$, $M = 2$ and the VS piecewise basis with a cosine spectral taper.

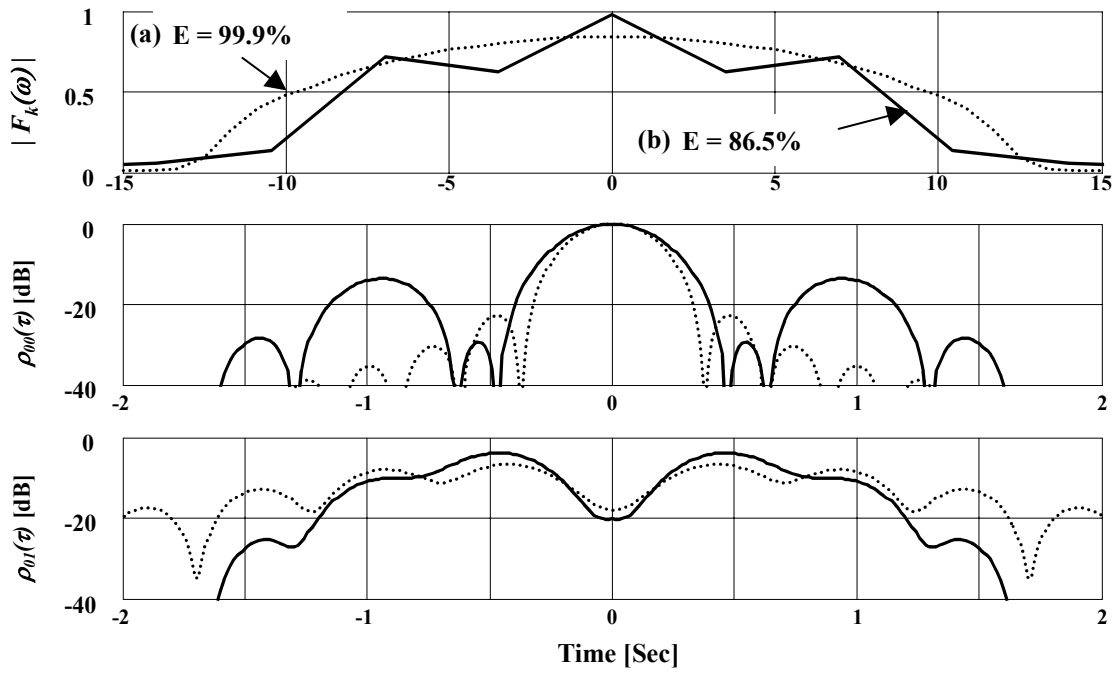

Figure 4-8. Windowed Brown Symbol, VS Piecewise Basis, Cosine Spectral Taper with $\Omega_0 = 8\pi$, $G_D = 1$ and $M = 2$. (a) $\sigma_k[T_w/2] = 4.7$ for Energy = 99.9% and (b) $\sigma_k[T_w/2] = 1.385$ for Energy = 86.5%

As time windowing is applied and energy levels are reduced, the symbol spectral response evolves from a cosine taper to a rectangular-like taper and the desired ACF and CCF sidelobe properties degrade. Specifically, the ACF main lobe width increases (poorer resolution) while its sidelobes experience a constructive-destructive process. The impact of truncating Brown symbols generated with a high dispersive gain is illustrated in Figure 4-9. Relative to data presented in Figure 4-8, all symbol specifications are maintained except $G_D = 40$ dB is used.

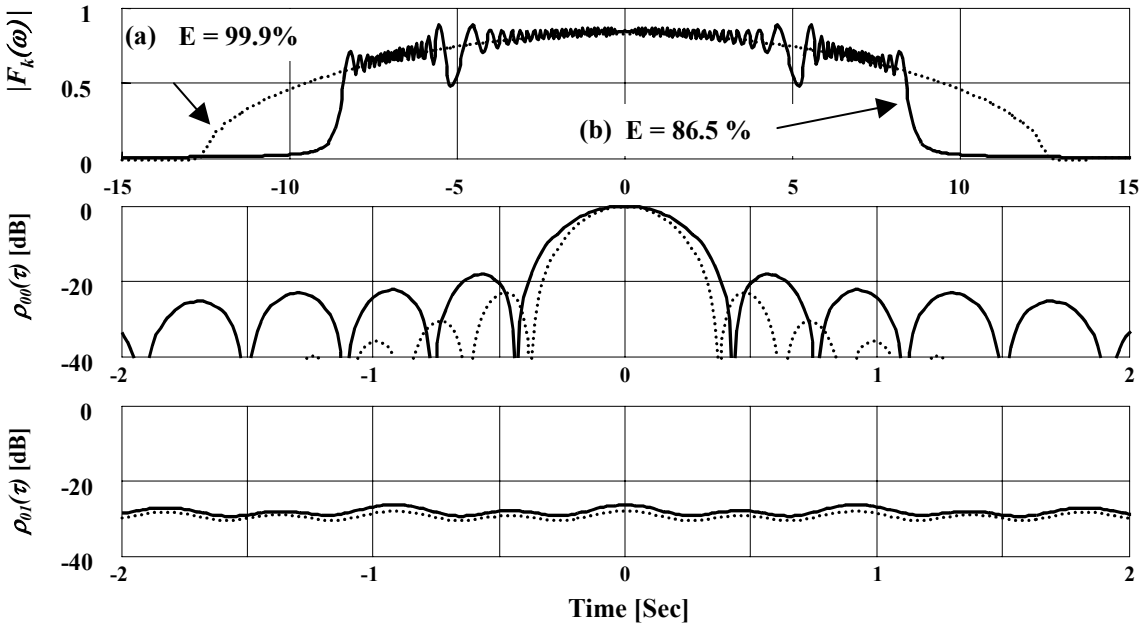

Figure 4-9. Windowed Brown Symbol, VS Piecewise Basis, Cosine Spectral Taper with $\Omega_0 = 8\pi$, $G_D = 40$ dB, $M = 2$. (a) $\sigma_k[T_w/2] = 4.7$ for Energy = 99.9% and (b) $\sigma_k[T_w/2] = 1.385$ for Energy = 86.5%

From the symbol spectral envelope perspective, $|F_k(\omega)|$ in Figure 4-9, the truncation has introduced sinusoidal structure across a narrower spectrum. The ACF $\rho_{00}(\tau)$ experiences some degradation in resolution and sidelobe levels, yet the overall structure is maintained. Likewise, the CCF $\rho_{01}(\tau)$ experiences minimal degradation and maintains good dispersive characteristics. The next scenario compares the effect of truncating VS piecewise-based Brown symbols generated using higher bandwidth and dispersive gain. In this case, the bandwidth is changed to $\Omega_0 = 40\pi$ with $G_D = 40$dB and representative results are shown in Figure 4-10.

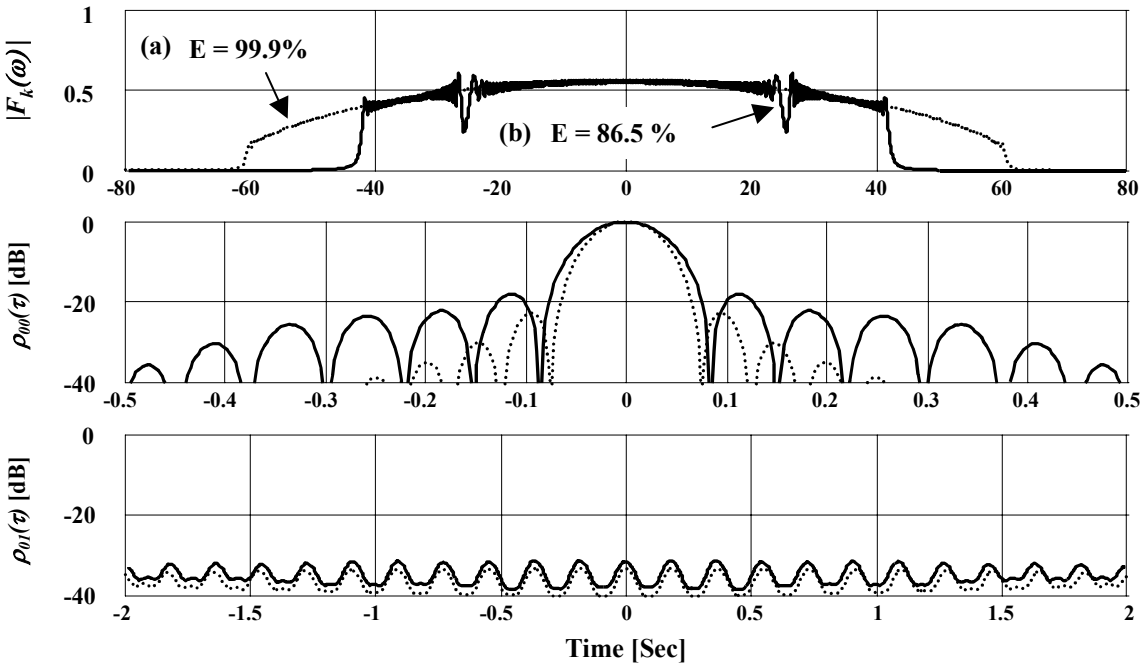

Figure 4-10. Windowed Brown Symbol, VS Piecewise Basis, Cosine Spectral Taper with $\Omega_0 = 40\pi$, $G_D = 40$ dB, $M = 2$. (a) $\sigma_k[T_w/2] = 4.7$ for Energy = 99.9% and (b) $\sigma_k[T_w/2] = 1.385$ for Energy = 86.5%

The ACF exhibits better compression than the previous cases since bandwidth is increased. Similar performance improvement in PCCL is realized with increasing bandwith. With truncation to the 86.5% energy level, spectral response $|F_k(\omega)|$ exhibits a similar rippling effect as experienced in the previous $\Omega_0 = 8\pi$, and $G_D = 40$ dB case. The ACF properties appear most sensitive to truncation, exhibiting a wider main lobe and higher sidelobe levels. The CCF in this case experiences similar minimal degradation as the previous scenario

In each of the time windowing scenarios, the symbol properties changed. The ACF sidelobe properties were most sensitive to truncation. Consequently, symbols must be generated at high bandwidth to accommodate the degradation in resolution encountered with the truncation. The energy level for windowing must be determined at

the application level and guided by the metrics of interest. The symbol design process provides flexibility to tailor symbol properties to meet specific requirements.

4.4 *Nonlinear Ambiguity Suppression (NLAS) Performance*

For NLAS concept demonstration, four uniquely coded, equal energy Brown symbols were generated. An *unambiguous* input signal $s_U(t)$ was created using symbol $f_0(t)$ and random noise $n(t)$, as shown in (4-7), with signal and noise power levels adjusted to achieve a –24.4 dB signal-to-noise ratio (SNR). Likewise, an *ambiguous* input signal $s_A(t)$ was created by adding two symbols to $s_U(t)$ as shown in (4-8). Signal power levels in $f_1(t)$ and $f_2(t)$ were adjusted to achieve a 0 dB SNR – the ambiguous signal power levels are +24.4 dB above the unambiguous signal power. The remaining symbol $f_3(t)$ was used by the NLAS processor to generate adaptive reserved code thresholds (ARCT) for suppressing ambiguous signal responses [14:2-35].

$$s_U(t) = f_0(t) + n(t) \tag{4-7}$$

$$s_A(t) = s_U(t) + \alpha f_1(t - t_1) + \beta f_2(t - t_2), \qquad \alpha, \beta \in C \qquad t_k \in \Re \tag{4-8}$$

The NLAS system performance is analyzed relative to symbol properties and NLAS effectiveness. At the symbol level, the effects of noise on correlation properties and the detection capability of unambiguous responses at two different correlation interference levels is analyzed. Similarly, at the NLAS processing level, the suppression of ambiguous energy levels and processing "overhead" is characterized. Performance is

bench marked relative to matched filtering. The NLAS analysis is conducted for Brown symbols generated with the new VS piecewise basis, the original CS piecewise basis, the sinusoidal basis and LFM. An equivalent time bandwidth (*TB*) product is used in all cases to establish "equivalence" in the symbol generation process. Time windowing is performed such that symbols possess 99.9% of the total energy. Given there are only two LFM symbols available for testing, a constant threshold (versus an ARCT) is used for LFM processing.

4.4.1 *Symbol Specifications for NLAS Demonstration*

Correlation statistics for the VS piecewise-based Brown symbols are shown in Table 4-4 with corresponding plots in Figure 4-11. The time functions, or Brown symbols, used for NLAS demonstration are shown in Figure 4-12.

Table 4-4. Correlation Statistics: VS Piecewise-Based Brown Symbol*s, M* = 4, E = 99.9%, G_D = 10 dB, TB = 7099 and Ω_o= 1058π

	PSL (dB)	ISL (dB)	PCCL (dB)	σ_{kk}^2	σ_{kl}^2
$\rho_{00}(\tau)$	-23.161	-18.901	-	8.93×10^{-7}	-
$\rho_{11}(\tau)$	-23.161	-18.901	-	8.93×10^{-7}	-
$\rho_{22}(\tau)$	-23.161	-18.901	-	8.93×10^{-7}	-
$\rho_{33}(\tau)$	-23.161	-18.901	-	8.93×10^{-7}	-
$\rho_{01}(\tau)$	-	-	-27.073	-	5.960
$\rho_{02}(\tau)$	-	-	-30.646	-	13.972
$\rho_{03}(\tau)$	-	-	-30.779	-	26.927

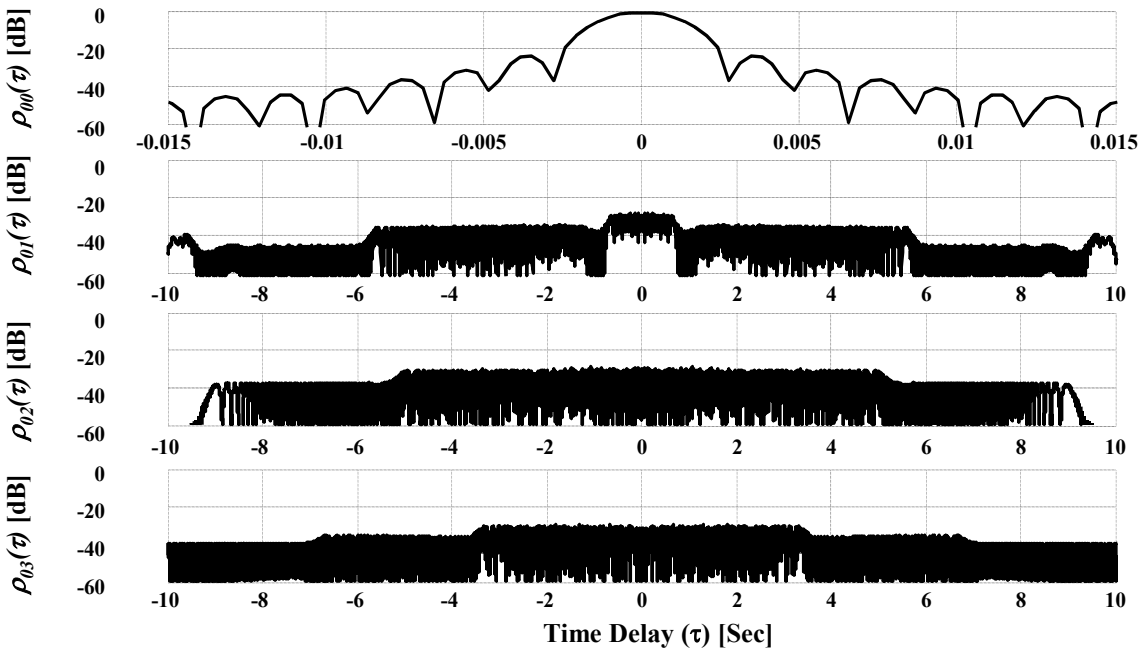

Figure 4-11. Brown Symbol Correlations, VS Piecewise Basis, for M = 4, E = 99.9%, G_D = 10 dB, TB = 7099 and Ω_o= 1058π

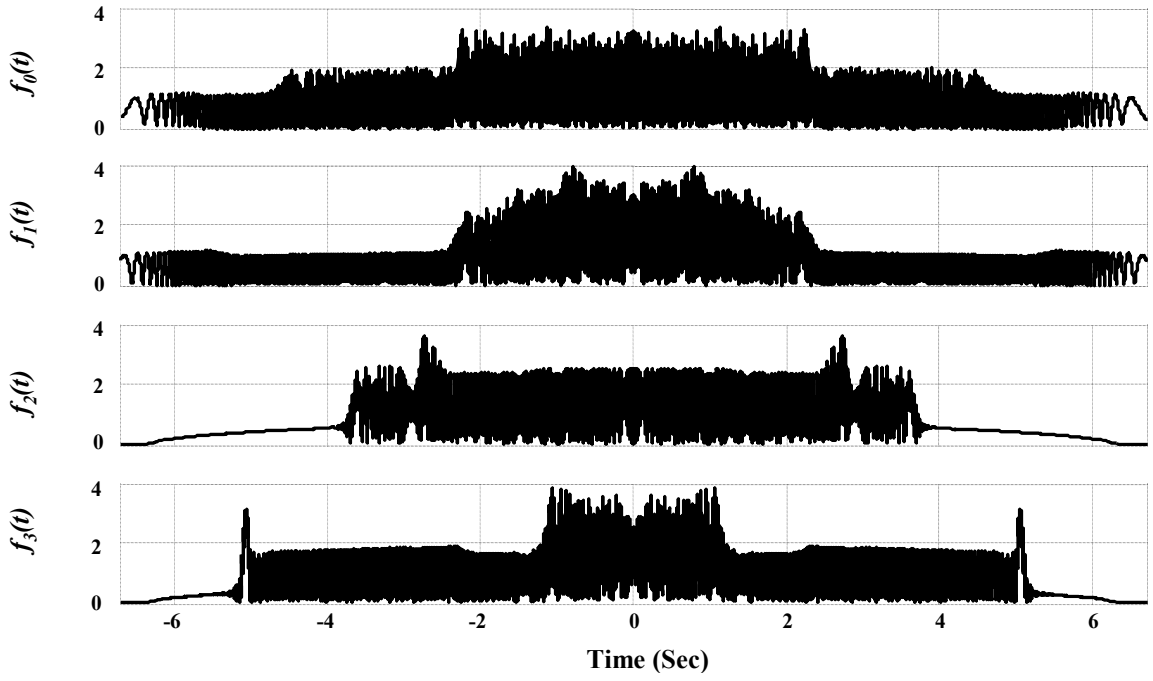

Figure 4-12. Brown Symbols, VS Piecewise Basis, for M = 4, E = 99.9%, G_D = 10 dB, TB = 7099, Ω_o= 1058π

4.4.2 *Symbol Performance: Noisy Channel with Matched Filter Detection*

The effect of additive noise on the correlation properties of $f_0(t)$ is analyzed by correlating $s_U(t)$ of (4-8) with $f_0(t)$ of Fig. (4-12), resulting in the matched filter response at SNR= -24.4 dB. Performance in a noisy channel provides an indication of ACF robustness when no ambiguous returns are present. The MF noisy channel response (solid line) shown in Figure 4-13 represents a "best case" scenario, i.e., the best response that can be achieved given no ambiguous signals are present. The noiseless ACF response (dashed line) is presented for reference. As ambiguous returns are introduced, the autocorrelation response would theoretically deteriorate from that shown in the figure. The range resolution afforded by the MF response in the noisy channel reflects minimal degradation for the noiseless case, i.e., the compressed pulse time duration at -4.0 db points of the dotted and solid lines is approximately equal. As indicated, PSL levels have increased by approximately 6.0 dB and the correlation response (solid line) outside the main lobe has much higher energy levels for time delays extending beyond the main lobe. The nature of the PSL levels changes based on noise realizations.

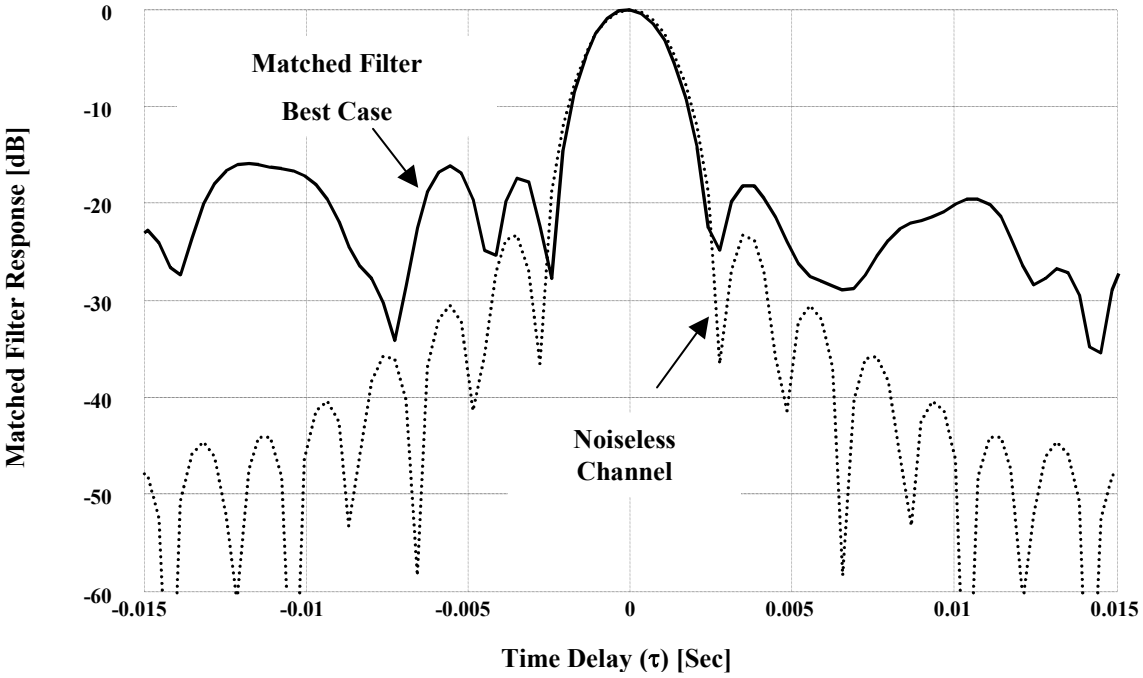

Figure 4-13. Matched Filter Noisy Channel Response for SNR = -24.4 dB (Solid Line) and Noiseless Autocorrelation Response (Dashed Line)

The MF noisy channel response of Figure 4-13 is redrawn in Figure 4-14 using a wider time delay scale to illustrate the correlation "noise floor" and "detection capability", Δ_D, of the MF response. The detection capability is the difference between the normalized (to "best case" peak response) response at $\tau = 0$ and the correlation noise floor. As indicated, the MF response exhibits a Δ_D of 12.10 dB.

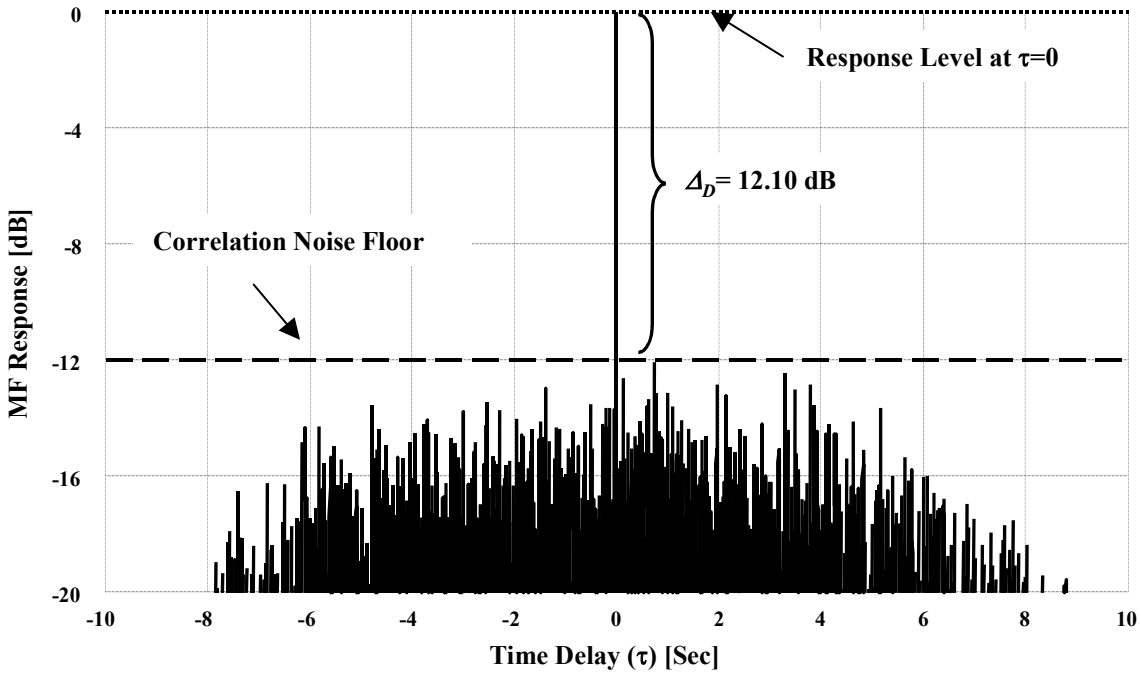

Figure 4-14. Matched Filter Noisy Channel Response for SNR = -24.4 dB with Correlation "Noise Floor" Indicated by Dashed Line

4.4.3 *Interference Effects on Matched Filter Detection Performance*

The next step in the symbol analysis process involves introduction of ambiguous signal responses per (4-8) (each scaled such that they are +24.4 dB above the desired unambiguous signal) and matched filtering (correlating) $f_0(t)$ with $s_A(t)$. In the first ambiguous case, the ambiguous responses are *completely overlapped* with the signal of interest by setting $t_k = 0$ in (4-8). The resultant MF response is shown in Figure 4-15 where the data has been normalized by the peak response of the best case MF scenario presented in Figure 4-14; this normalization is introduced to show the effective increase in the correlation "noise floor" (energy levels). The detection capability, Δ_D, is the difference between the normalized (to "best case" MF peak response) response at $\tau = 0$ and the correlation noise floor. As indicated, the MF response with Δ_D = - 1.42 dB does not have a clearly discernable peak which can be attributed to the desired unambiguous

signal, i.e., the unambiguous signal is undetectable by simple matched filtering; the "negative" sign implies that the cross correlation levels are higher than the response of interest.

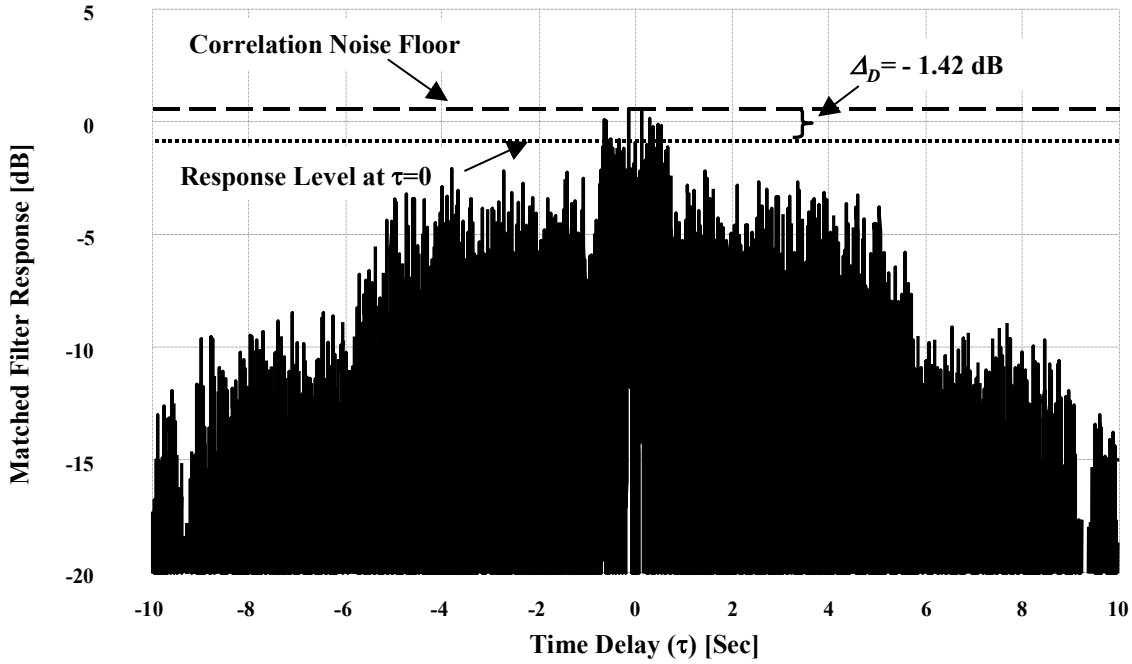

Figure 4-15. Match Filter Response for Completely Overlapping Ambiguous Scenario – Two Ambiguous Signals Present at +24.4 dB above Unambiguous Signal.

Although the VS piecewise-based Brown symbols were designed with PCCL's of approximately -30 dB, the +24.4 dB power differential between $f_0(t)$ and $\beta f_2(t)$ has increased the PCCL of $\rho_{02}(\tau)$ to effectively -6.0 dB. Similarly, the effective PCCL of $\rho_{01}(\tau)$ has increased to -3.0 dB. These higher effective cross-correlation levels raise the -12.10 dB peak correlation "noise floor" of Figure 4-14 to the 0.575 dB level illustrated in Figure 4-15, rendering the match filtering process totally ineffective for detecting the signal of interest. Ideally, the MF response at the $\tau = 0$ in Figure 4-15 should only contain contributions from the unambiguous focused response of $f_0(t)$. Given the Brown

symbols are designed to be mutually dispersive in terms of their cross-correlation responses, $f_0(t)$ with $f_1(t)$ and $f_0(t)$ with $f_2(t)$, the MF response of Figure 4-15 should contain minimal ambiguous energy at $\tau = 0$; the +24.4 dB power differential of this scenario has mitigated all advantage provided by matched filtering.

In the second ambiguous case considered, cross-correlation interaction and interference levels are controlled by *partially overlapping* the unambiguous and ambiguous signals. This is done by adjusting ambiguous signal time delays such that $t_1 = 0.5T$ and $t_2 = -0.5T$ in (4-8) where T is the transmitted pulse duration. Ambiguous signal power levels were maintained from the previous case at +24.4 dB above the desired unambiguous signal level. The MF response to the ambiguous signal in this case is shown in Figure 4-16. The MF autocorrelation response of $f_0(t)$ at $\tau = 0$ still contains contributions from $\alpha f_1(t)$ and $\beta f_2(t)$, yet the cross-correlation energy available from each ambiguous symbol for the "combined" process is less than the previous overlapped case. Given the complex nature of the processing involved, there is no way of predicting that the response at $\tau = 0$ will be more or less strong than the first case. As indicated in Figure 4-16, the peak correlation "noise floor" has decreased to -2.90 dB and the compressed response for $f_0(t)$ is more visible with detection capability $\Delta_D = 4.04$ dB. If the ambiguous cross-correlation responses were completely flat (ideal design), the correlation "noise floors" of the displaced and completely overlapping scenarios would be approximately equal. If the unambiguous and ambiguous signals are not overlapped at all, the MF process can effectively detect the unambiguous response as a function of received SNR.

Table 4-5 is a summary of the MF responses for the VS piecewise-based Brown symbols; No Detectable Response (NDR) is referenced in the table to categorize filter responses without a discernable peak.

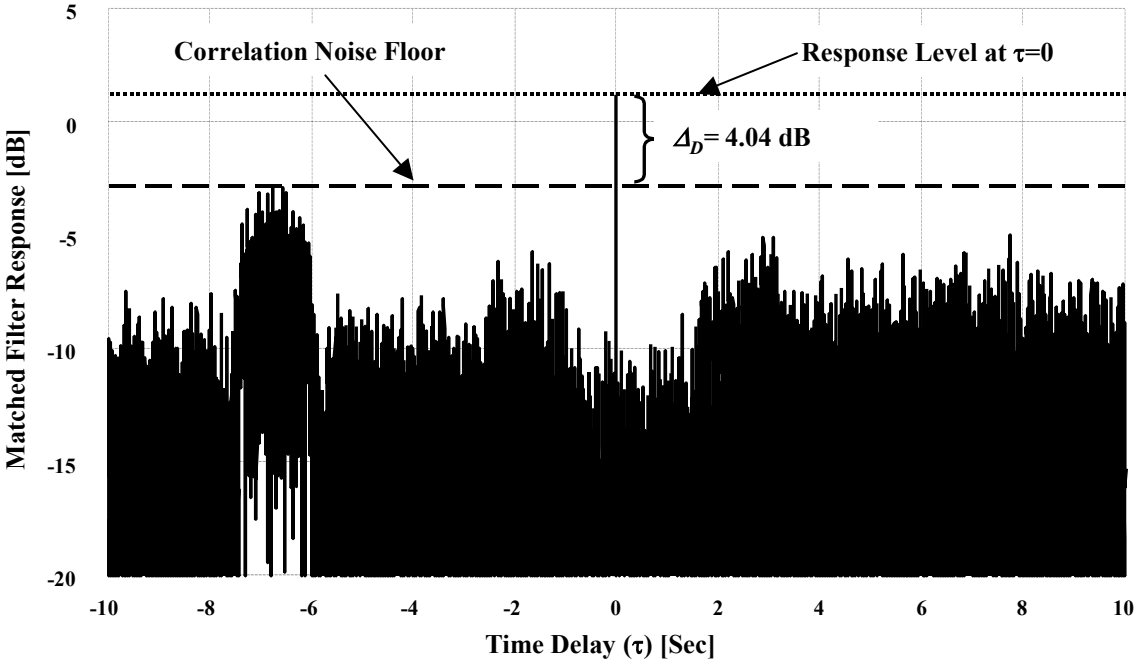

Figure 4-16. Match Filter Response for Partially Overlapping Ambiguous Scenario – Two Ambiguous Signals Present at +24.4 dB above Unambiguous Signal.

Table 4-5. Summary: MF Response for VS Piecewise-Based Brown Symbols

Metrics	Noiseless Channel	Noisy Channel Best Case	Noisy Channel $t_k = 0$	Noisy Channel $t_k = \pm 0.5T$
Resolution (Sec)	2.57×10^{-3}	2.44×10^{-3}	NDR	NDR
PSL (dB)	-23.16	-17.45	-	-
"Noise Floor" (dB)	-	-12.10	0.58	-2.90
Peak Response at $\tau = 0$ (dB)	0.00	0.00	-2.00	1.14
Δ_D (dB)	23.16	12.10	-1.42	4.04

4.4.4 *NLAS Performance in Noisy Channel*

A "best case" NLAS performance baseline is first established by applying the unambiguous signal $s_U(t)$ of (4-8) to an NLAS processor channel dedicated to isolating the unambiguous response. As in previous testing, the SNR $s_U(t)$ was maintained at -24.4 dB. The resultant "best case" output represents the expected NLAS output under ambiguous signal $s_A(t)$ input conditions with the NLAS processor *perfectly* removing ambiguous signal responses. To generate the "best case" results with $s_U(t)$ as the input, the NLAS processor uses a constant "infinite" threshold to ensure no energy (only desired energy is present) is hole-punched during NLAS processing. A comparison of the "best case" output with the MF output provides a "finger print" (coloration effects) for the NLAS processor. The final channel output from the "best case" scenario is used as a benchmark for system. Comparison of subsequent NLAS results with "best case" performance provides a means for determining how much desired (unambiguous) energy is lost and how much undesired (ambiguous) energy remains in the final NLAS processor output. The "best case" NLAS system benchmark is shown in Figure 4-17 along with the noiseless channel ACF (dotted line) for reference.

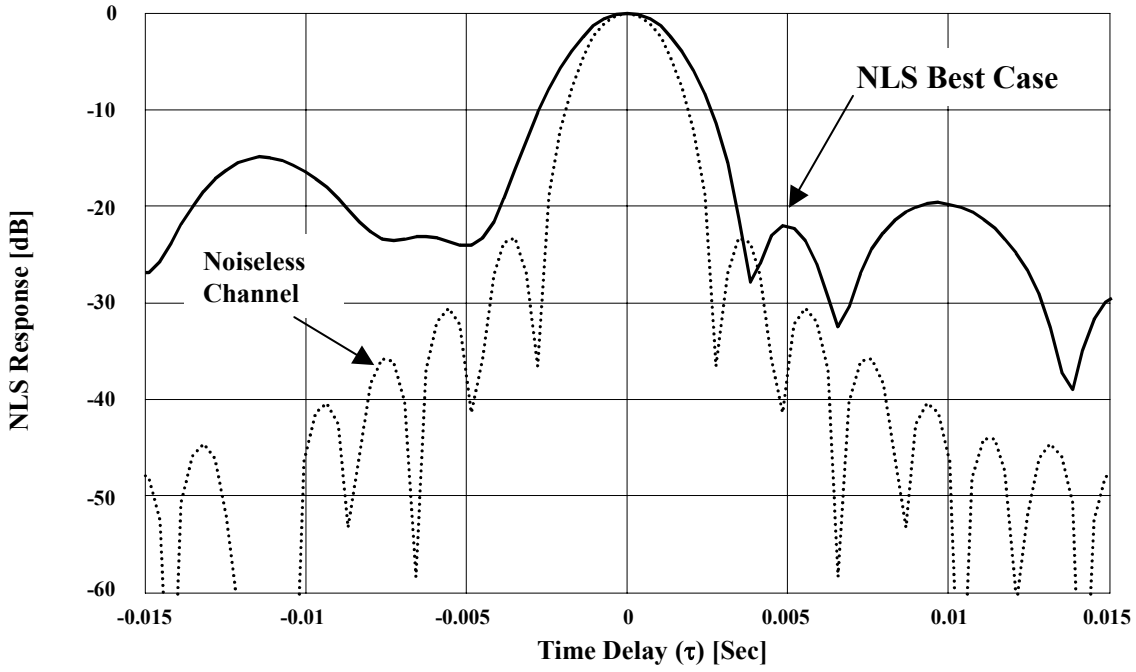

Figure 4-17. "Best Case" NLAS Performance for SNR = -24.4 dB, VS Piecewise-Based Brown symbols, Infinite NLAS Threshold.

As indicated in Figure 4-17, NLAS processing clearly impacts ACF resolution, even under these "best case" conditions. This degradation (coloration) is primarily introduced by the focusing and defocusing filter operations within the NLAS process since the additive channel noise mainly affects sidelobe structure. Although the width of the main lobe has increased, the PSL level remains at –23 dB. The "best case" NLAS response is redrawn using a larger time scale in Figure 4-18 and exhibits a correlation "noise floor" of -10.5 dB with detection capability Δ_D of –10.50 dB. In all the NLAS scenarios, the detection capability is the difference between the normalized (to "best case" NLAS peak response) response at $\tau = 0$ and the correlation noise floor. The MF correlation "noise floor" shown in Figure 4-14 is -12.05 dB, or 1.55 dB lower the "best case" NLAS response.

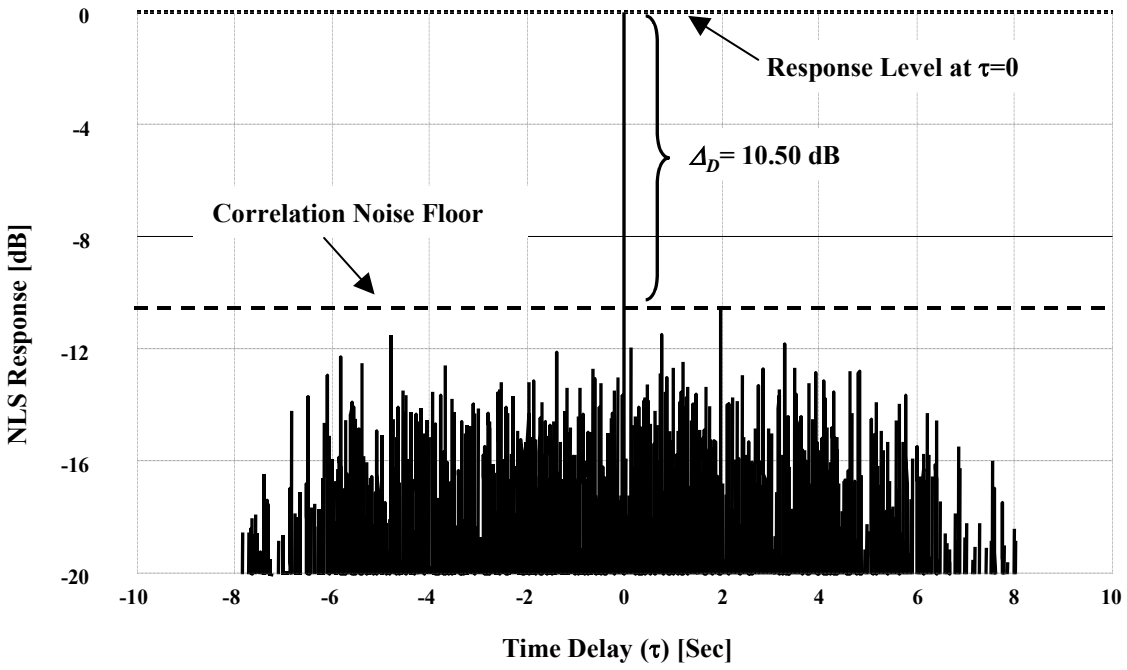

Figure 4-18. Correlation "Noise Floor" for "Best Case" NLAS Performance with SNR = -24.4 dB, VS Piecewise-Based Brown Symbols, Infinite NLAS Threshold.

4.4.5 *Interference Effects on NLAS Detection Performance*

After benchmarking NLAS performance with the "best case" scenario, the *completely overlapped* ambiguous signal $s_A(t)$, $t_k = 0$ in (4-8) per previous testing, was input into the NLAS processor. NLAS processing coloration is established using $s_A(t)$ as the input signal and the threshold set to "infinity" such that no NLAS suppression occurs. This output provides an indication of ambiguous energy in the system as induced by symbol correlation properties and filter coloration. The resultant NLAS unsuppressed output for the completely overlapped ambiguous input scenario is shown in Figure 4-19. The difference between the peak correlation level at $\tau \neq 0$ in the unsuppressed output and the suppressed output is used to quantify the ambiguous energy suppression performance of the NLS system.

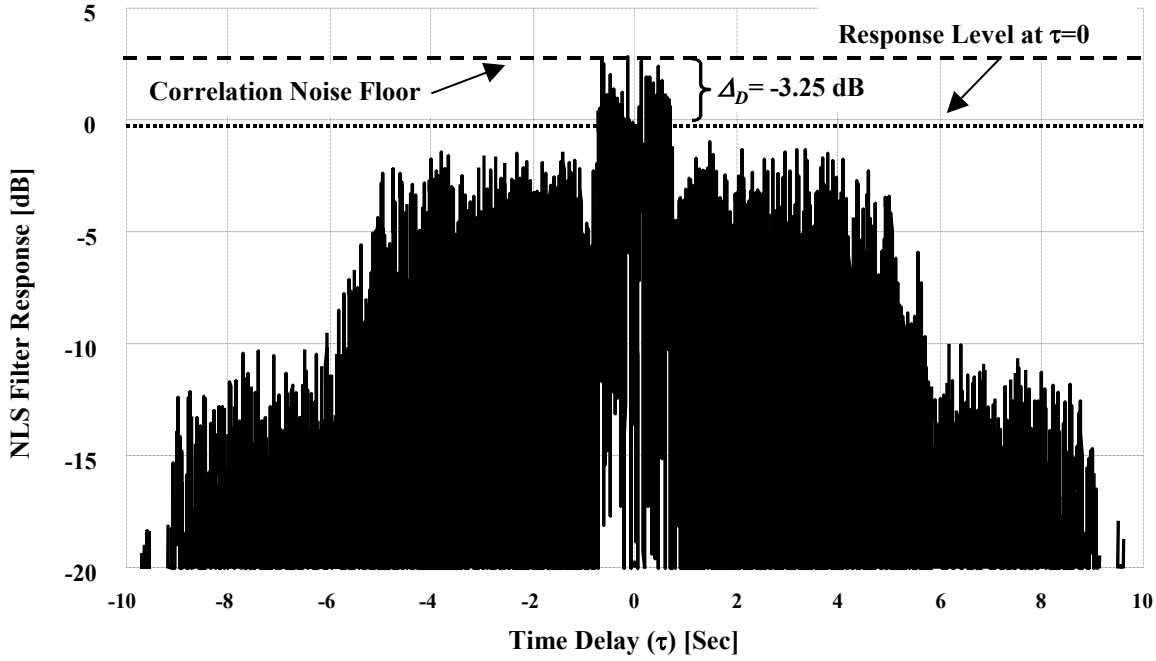

Figure 4-19. NLAS *Unsuppressed* Output (Infinite Threshold) for *Completely Overlapped* Ambiguous Input.

As indicated in Figure 4-19, the peak correlation "noise floor" is at 2.75 dB and the peak response is undetectable with a $\Delta_D = -3.25$ dB The "noise floor" has contributions from symbol correlation interactions and processor filter coloration. A comparison of the correlation "noise floor" of Figure 4-19 with the corresponding MF response in Figure 4-15 indicates a 2.18 dB change (coloration) in the ambiguous energy response. Finally, $s_A(t)$ is applied to the NLAS processor with adaptive reserved code thresholding applied. The NLAS suppressed output with adaptive thresholding applied is shown in Figure 4-20. As indicated, the correlation "noise floor" of the NLAS suppressed response is at -10.75 dB. The difference between the NLS "best case" peak (0 dB) and normalized *suppressed* response at $\tau = 0$ is introduced as Δ_P, the ACRT processing cost. A negative quantity in this metric indicates the hole-punching of "good" responses during

the ACRT operation. Similarly, a positive quantity for Δ_P is representative of ineffective suppression of ambiguous responses. As indicated in Figure 4-20, 0.75 dB of the unambiguous signal was lost during the thresholding process.

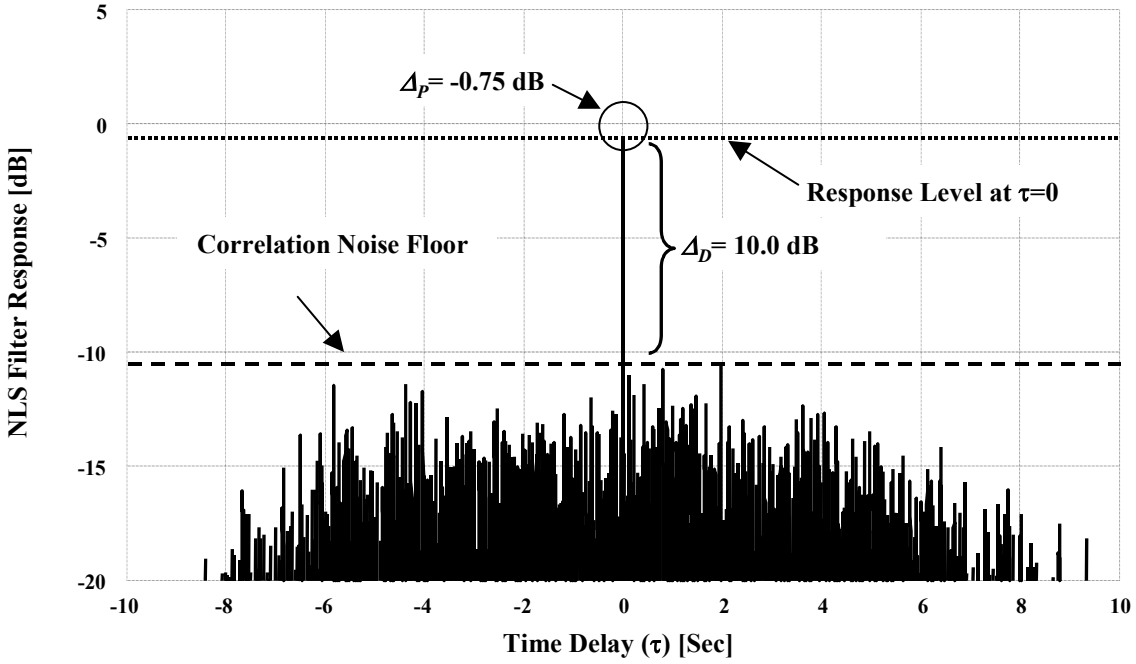

Figure 4-20. NLAS *Suppressed* Output (Adaptive Reserved Code Threshold) for *Completely Overlapped* Ambiguous Input.

Following the MF interference analysis process of Section 4.4.3, cross-correlation interaction and interference levels are controlled by *partially overlapping* the unambiguous and ambiguous signals. The change in interference level is simulated by by adjusting ambiguous signal time delays such that $t_1 = 0.5T$ and $t_2 = -0.5T$ in (4-8) where T is the transmitted pulse duration. The NLAS response to (4-8) without NLAS suppression applied is shown in Figure 4-21.

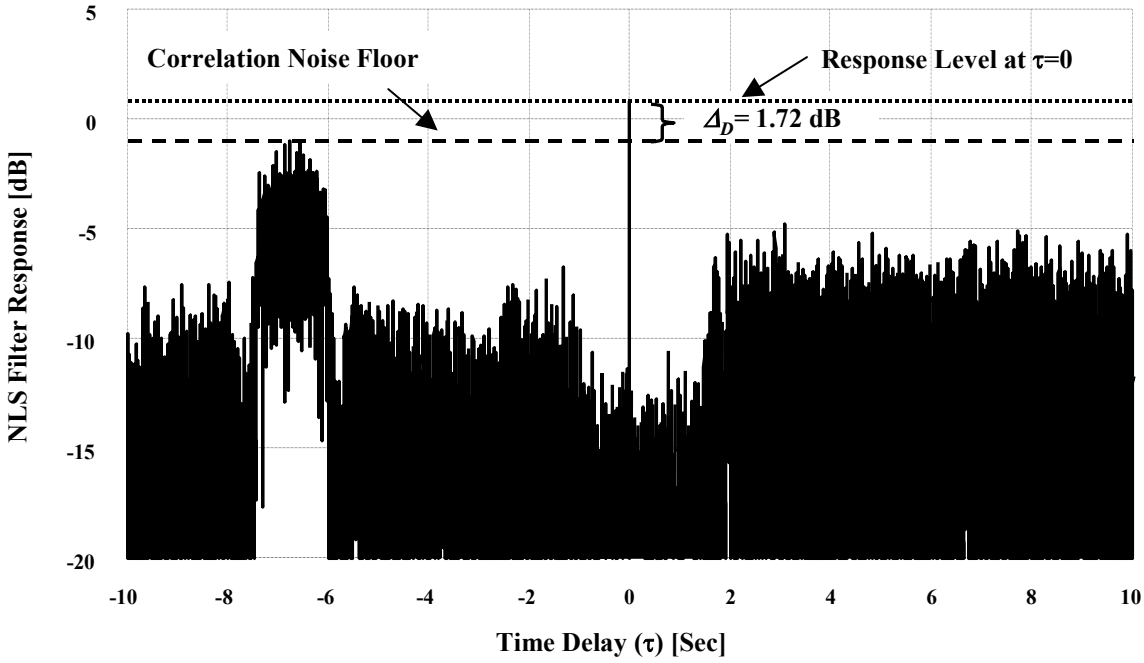

Figure 4-21. NLAS *Unsuppressed* Output (Infinite Threshold) for *Partially Overlapped* Ambiguous Input.

As indicated in Figure 4-21, the peak correlation "noise floor" is at -1.02 dB with a detection capability $\Delta_D = 1.72$ dB. Even with the displacement in ambiguous signal locations (varying interference levels), the contributions forming the ambiguous peaks (and filter coloration) in the autocorrelation response of $f_0(t)$ at $\tau = 0$ is evident with a peak response of 0.70 dB above the "NLAS Best Case". The NLAS suppressed output, using adaptive reserved code thresholding, for the *partially overlapping* ambiguous input signal is shown in Figure 4-22. As indicated, the peak correlation "noise floor" is now at –11.25 dB and the desired unambiguous response is clearly visible.

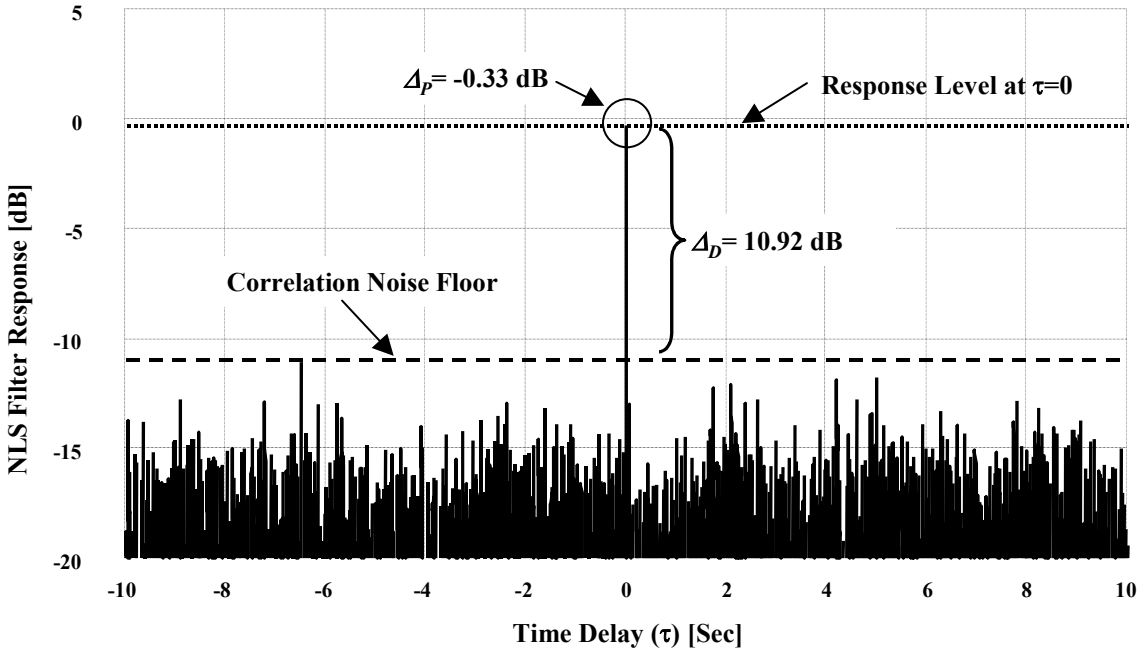

Figure 4-22. NLAS *Suppressed* Output (Adaptive Reserved Code Threshold) for *Partially Overlapped* Ambiguous Input, Normalized by NLAS "Best Case" Response.

4.4.6 *NLAS Processing Cost*

A comparison between the NLAS "best case" and final NLAS system response to $s_U(t)$, in both the completely and partially overlapped scenarios, is considered. Differences and/or similarities resulting from this analysis help characterize the NLAS effectiveness when using adaptive reserved thresholding – effectiveness is fundamentally driven by symbol cross correlation characteristics. Thresholding effectiveness is determined by the ability to hole-punch (null-out) as much undesired focused energy as possible while simultaneously retaining as much dispersed signal as possible. The final NLAS system response for the completely overlapped ambiguous signal scenario, along with NLAS "best case" results, is show in Figure 4-23. The difference in the peak responses at $\tau = 0$ is 0.75 dB, indicating the final energy in the desired response due to $f_0(t)$ at the NLAS

suppressed output is only marginally reduced relative to "best case" performance – desired unambiguous $f_0(t)$ signal energy was well-preserved throughout the NLAS suppression process and minimal energy was "lost."

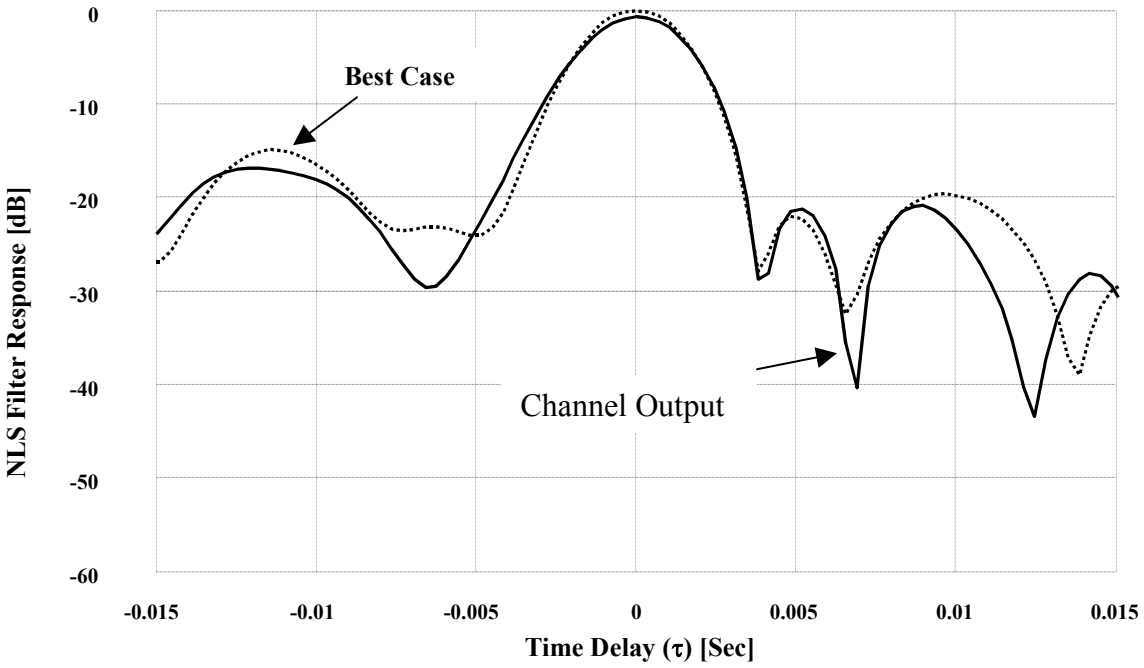

Figure 4-23. NLAS Comparison: "Best Case" (Dashed Line) versus Suppressed NLAS Performance (Solid Line) for *Completely Overlapped* Ambiguous Input

An equivalent comparison was made for the partially overlapped ambiguous input with results presented in Figure 4-24. In this case, the difference in the peak responses at $\tau = 0$ is only 0.33 dB, once again indicating that the final energy in the response due to $f_0(t)$ at the NLAS suppressed output is only marginally reduced relative to "best case" performance. A summary of NLAS processing results and associated metrics for ambiguous cases using VS piecewise-based Brown Symbols is provided in Table 4-6.

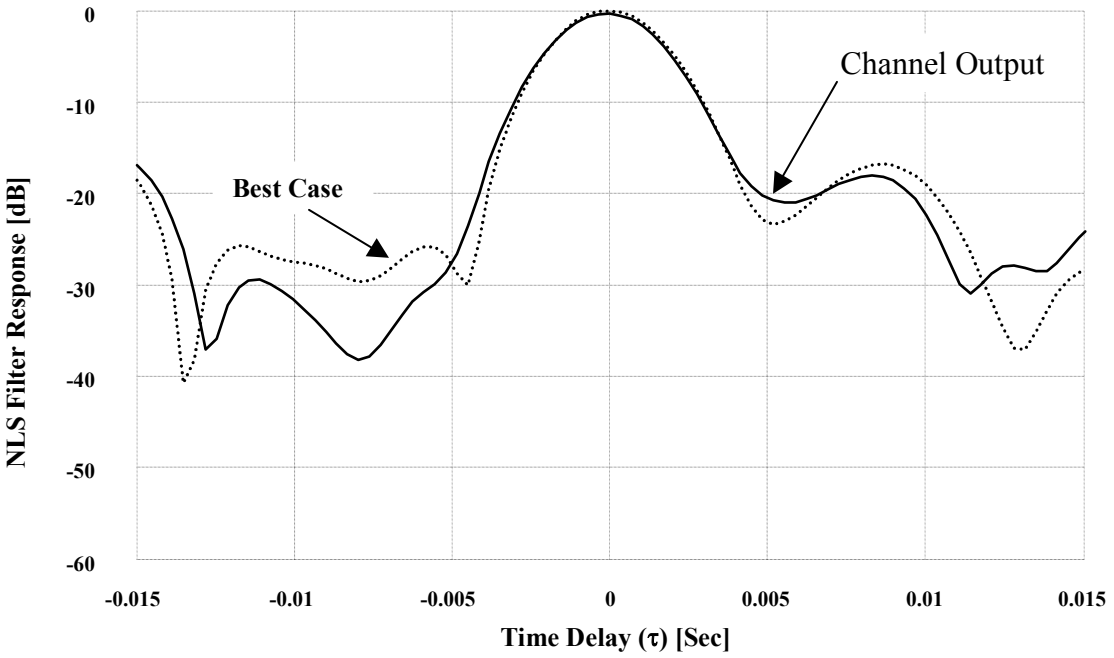

Figure 4-24. NLAS Comparison: "Best Case" (Dashed Line) versus Suppressed NLAS Performance (Solid Line) for *Partially Overlapped* Ambiguous Input

Table 4-6. NLAS Output Summary: VS Piecewise-Based Brown symbols with Channel SNR = -24.4 dB

Metrics	"Best Case"	No NLAS $t_k = 0$	With NLAS $t_k = 0$	No NLAS $t_k = \pm 0.5T$	With NLAS $t_k = \pm 0.5T$
Resolution (Sec)	3.53×10^{-3}	NDR	$3.73\times10^{-}$	3.52×10^{-3}	3.86×10^{-3}
PSL (dB)	-23.00	-	-16.12	-13.42	-17.70
"Noise Floor" (dB)	-10.5	2.75	-10.75	-1.02	-11.25
Ambiguity Supp.	-	-	13.50	-	10.23
Peak Response (dB)	0.00	-0.50	-0.75	0.70	-0.33
Δ_D (dB)	10.5	-3.25	10.00	1.72	10.92
Δ_P (dB)	-	-	-0.75	-	-0.33

4.4.7 *NLAS Performance for Other Symbols*

NLAS performance using LFM, sinusoidal-based Brown symbols and CS piecewise-based Brown symbols is documented in the following manner:

a) LMF symbol specifications are shown in Table 4-7 with associated MF and NLAS response statistics provided in Table 4-8 and Table 4-9, respectively

b) Sinusoidal-based Brown symbol specifications are shown in Table 4-10 with associated MF and NLAS response statistics provided in Table 4-11 and Table 4-12, respectively.

c) CS piecewise-based Brown symbol specifications are shown in Table 4-13 with associated MF and NLAS statistics provided in Table 4-14 and Table 4-15, respectively.

In general, the following performance trends were observed across all symbols employed in the NLAS system:

a) NLAS processing provided for an average of +8.50 dB improvement in signal detection performance for the *completely overlapped* scenario and +6.39 dB for the *partially overlapped* scenario compared to traditional MF.

b) Piecewise-based Brown symbols provided equivalent detection performance to LFM waveforms with NLAS processing. LMF performance was superior to Brown symbols using traditional MF.

c) Range resolution performance degraded with NLAS processing resulting from coloration induced by the focusing-defocusing operation.

d) ARCT operation effectively preserved the unambiguous response of interest with worst case lost at -0.75 dB. Similarly, the hole-punching operation effectively removed undesired signals with worst case being +0.29 dB; if the undesired signals were completely removed a 0 dB suppressed peak response would be ideally realized.

e) The NLAS technique effectively suppressed ambiguous energy levels in all the processed waveforms. The suppression performance improved with introduction of ambiguous responses for all symbols employed in the system, with the exception of sinusoidal based Brown symbols.

A comparative summary of the symbol performance is shown in Table 4-16 to Table 4-18.

Table 4-7. Correlation Statistics of LFM symbols: $M = 2$, $E > 99\%$, $TB = 7093$, $\Omega_o = 1058\pi$

	PSL (dB)	ISL (dB)	PCCL (dB)	σ_{kk}^2	σ_{kl}^2
$\rho_{00}(\tau)$	-13.31	-6.83	-	2.68×10^{-3}	-
$\rho_{11}(\tau)$	-13.31	-6.83	-	2.68×10^{-3}	-
$\rho_{01}(\tau)$	-	-	-38.96	-	59.98

Table 4-8. Matched Filter Response for LFM Symbols

Metrics	Noiseless Channel	Noisy Channel Best Case	Noisy Channel $t_k = 0$	Noisy Channel $t_k = \pm 0.5T$
Resolution (Sec)	1.89×10^{-3}	1.99×10^{-3}	2.39×10^{-3}	1.89×10^{-3}
PSL (dB)	-13.31	-15.77	-6.92	-8.35
"Noise Floor" (dB)	-	-12.54	-6.66	-6.65
Peak Response at $\tau=0$ (dB)	-	0.00	1.57	1.83
Δ_D (dB)	-	12.54	8.23	8.48

Table 4-9. NLAS Output for LFM Symbols: Channel SNR = -24.4 dB

Metrics	Best Case	No NLAS $t_k = 0$	With NLAS $t_k = 0$	No NLAS $t_k = \pm 0.5T$	With NLAS $t_k = \pm 0.5T$
Resolution (Sec)	2.0×10^{-3}	$2.7\times10^{-}$	1.9×10^{-3}	2.1×10^{-3}	2.0×10^{-3}
PSL (dB)	-15.95	-7.75	-15.92	-9.32	-13.33
"Noise Floor" (dB)	-10.70	-5.06	-10.91	-6.57	-11.05
Ambiguity Supp. (dB)	-	-	5.84	-	4.48
Peak Response (dB)	0.00	1.84	4.00e-3	0.96	4.00e-3
Δ_D (dB)	10.70	6.90	10.91	7.53	11.05
Δ_P (dB)	-	-	4.0×10^{-3}	-	4.0×10^{-3}

Table 4-10. Correlation Statistics of Sinusoidal-Based Brown Symbols: $M = 4$, $E > 99\%$, $G_D = 1000$, $TB = 7153$, $\Omega_o = 78\pi$

	PSL (dB)	ISL (dB)	PCCL (dB)	σ_{kk}^2	σ_{kl}^2
$\rho_{00}(\tau)$	-23.02	-18.83	-	1.64×10^{-4}	-
$\rho_{11}(\tau)$	-23.02	-18.83	-	1.64×10^{-4}	-
$\rho_{22}(\tau)$	-23.02	-18.83	-	1.64×10^{-4}	-
$\rho_{33}(\tau)$	-23.02	-18.83	-	1.64×10^{-4}	-
$\rho_{01}(\tau)$	-	-	-9.87	-	2666.7
$\rho_{02}(\tau)$	-	-	-12.00	-	2666.7
$\rho_{03}(\tau)$	-	-	-10.94	-	2666.7

Table 4-11. Matched Filter Response for Sinusoidal-Based Brown Symbols

Metrics	Noiseless Channel	Noisy Channel Best Case	Noisy Channel $t_k = 0$	Noisy Channel $t_k = \pm 0.5T$
Resolution (Sec)	4.81×10^{-2}	3.55×10^{-2}	NDR	NDR
PSL (dB)	-23.02	-16.91	-	-
"Noise Floor" (dB)	-	-12.20	14.74	14.53
Peak Response at $\tau=0$ (dB)	-	0.00	8.60	6.50
Δ_D (dB)	-	12.20	-6.14	-8.03

Table 4-12. NLAS Output for Sinusoidal-Based Brown Symbols: Channel SNR = -24.4 dB

Metrics	Best Case	No NLAS $t_k = 0$	With NLAS $t_k = 0$	No NLAS $t_k = \pm 0.5T$	With NLAS $t_k = \pm 0.5T$
Resolution (Sec)	5.09×10^{-2}	NDR	NDR	NDR	NDR
PSL (dB)	-	-	-	-	-
"Noise Floor" (dB)	-13.18	15.00	1.83	14.76	0.33
Ambiguity Supp. (dB)	-	-	13.17	-	14.43
Peak Response (dB)	0.00	10.90	0.29	6.25	-0.64
Δ_D	13.18	-4.10	-1.54	-8.51	-0.97
Δ_P	-		0.29	-	-0.64

Table 4-13. Correlation Statistics of CS Piecewise-Based Brown Symbols: $M = 4$, $E > 99\%$, $G_D = 10$, $TB = 7098$, $\Omega_o = 1000\pi$

	PSL (dB)	ISL (dB)	PCCL (dB)	σ_{kk}^2	σ_{kl}^2
$\rho_{00}(\tau)$	-23.00	-18.76	-	1.0×10^{-6}	-
$\rho_{11}(\tau)$	-23.00	-18.76	-	1.0×10^{-6}	-
$\rho_{22}(\tau)$	-23.00	-18.76	-	1.0×10^{-6}	-
$\rho_{33}(\tau)$	-23.00	-18.76	-	1.0×10^{-6}	-
$\rho_{01}(\tau)$	-	-	-26.36	-	15.01
$\rho_{02}(\tau)$	-	-	-29.62	-	26.66
$\rho_{03}(\tau)$	-	-	-27.64	-	26.66

Table 4-14. Matched Filter response for CS Piecewise-Based Brown Symbols

Metrics	Noiseless Channel	Noisy Channel Best Case	Noisy Channel $t_k = 0$	Noisy Channel $t_k = \pm 0.5T$
Resolution (Sec)	2.73×10^{-3}	2.69×10^{-3}	NDR	2.84×10^{-3}
PSL (dB)	-22.54	-14.28	-	-7.35
"Noise Floor" (dB)	-	-11.93	3.59	-0.79
Peak Response at $\tau=0$ (dB)	-	0.00	-0.75	1.04
Δ_D (dB)	-	11.93	-4.34	1.83

Table 4-15. NLAS Output for CS Piecewise-Based Brown Symbols: Channel SNR = -24.4 dB

Metrics	Best Case	No NLAS $t_k = 0$	With NLAS $t_k = 0$	No NLAS $t_k = \pm 0.5T$	With NLAS $t_k = \pm 0.5T$
Resolution (Sec)	3.90×10^{-3}	NDR	3.76×10^{-3}	4.74×10^{-3}	3.97×10^{-3}
PSL (dB)	-19.11	-	-19.95	-9.29	-16.58
"Noise Floor" (dB)	-11.08	4.23	-11.22	-0.96	-11.25
Ambiguity Supp.	-	-	15.46	-	10.28
Peak Response (dB)	0.00	-0.55	-0.20	1.09	-0.36
Δ_D (dB)	11.08	-4.78	11.02	2.05	10.89
Δ_P (dB)	-	-	-0.20	-	-0.36

Table 4-16. Comparison of Detection Capability and NLAS Processing Cost for *Completely Overlapped* Scenario ($t_k = 0$) (Relative to peak response)

	LFM	Sinusoidal	CS Piecewise	VS Piecewise
MF Δ_D (dB)	8.23	-6.14	-4.34	-1.42
NLAS Δ_D (dB)	10.91	-1.54	11.02	10.00
Ambiguity Supp.(dB)	5.84	13.17	15.46	13.50
Processing Cost Δ_P (dB)	.004	0.29	-0.20	-0.75

Table 4-17. Comparison of Detection Capability and NLAS Processing Cost for *Partially Overlapped* Scenario Scenario ($t_k = \pm 0.5T$). (Relative to Peak Response)

	LFM	Sinusoidal	CS Piecewise	VS Piecewise
MF Δ_D (dB)	8.48	-8.03	1.83	4.04
NLAS Δ_D (dB)	11.05	-0.97	10.89	10.92
Ambiguity Supp.(dB)	4.48	14.43	10.28	10.23
Processing Cost Δ_P (dB)	.004	-0.64	-0.36	-0.33

Table 4-18. Signal Detection Performance Improvement Using NLAS over MF

Scenario	LFM	Sinusoidal	CS Piecewise	VS Piecewise	Avg Imp
Overlapped (dB)	2.68	4.60	15.36	11.42	8.51
Partially Overlapped (dB)	2.57	7.06	9.06	6.88	6.39

CHAPTER 5. CONCLUSIONS AND RECOMMENDATIONS

5.1 *Introduction*

Chapter 5 provides a summary of the research results and contributions. Efforts to improve ambiguity suppression using NLAS are discussed and recommendations for future research provided.

5.2 *Restatement of Research Goal*

As stated in Section 1.3, the research goals include:

1. The design, synthesis and characterization of new Brown symbols generated with a variable slope piecewise basis functions.
2. Demonstration of the impacts associated with deviating from Brown's prescribed design process.
3. Characterizing the effect that time windowing (truncation) band limited Brown symbols has on NLAS implementation and performance.
4. Characterizing NLAS detection and ambiguity suppression effectiveness using new Brown symbols and subsequent comparison with previously developed symbols.

5.3 *Conclusions*

5.3.1 *Variable Slope (VS) Piecewise Basis Functions*

By considering the rms time duration of correlation functions, the Brown symbol theory provides a design methodology that decouples and optimizes the compression (envelope attributes) and dispersion (phase attributes) property of symbols. Although the rms time duration metric is widely used to characterize signal properties and provides a convenient theoretical approach to designing mutually dispersive symbols, the codes suitable for NLAS applications must also possess good performance in terms of the Peak Cross-Correlation Level (PCCL) metric. In categorizing symbols as either acceptable or unacceptable for NLAS applications, waveform dispersive properties must be viewed in light of both the rms time duration and PCCL metrics. The rms time duration of correlation functions alone is insufficient for basing a final decision. Chapter IV considered the design of Brown symbols using Variable Slope (VS) piecewise basis functions to improve PCCL performance while preserving waveform rms time duration properties. This approach led to implementation of sub-optimal basis functions using an otherwise optimal cosine spectral taper. As a result, the PCCL performance improved by 7.5 dB relative to optimal symbols generated using sinusoidal basis functions, with degradation to *equally* mutual dispersive properties captured by the rms metric. The compromise of optimality in the dispersion metric was justified by the flexibility offered in the dispersive gain parameter G_D to control mutual dispersion. The properties of piecewise based symbols having increased bandwidth (Figure 4-5) added another dimension for optimizing Brown symbol PCCL performance. The improvement achieved in cross-correlation sidelobe levels (which is linked to phase function design)

did not affect the waveform compressive properties (which are linked to envelop design); this is a result of the decoupled design approach offered by the graceful theory.

5.3.2 *Time Windowing Brown Symbols*

Brown symbols generated with larger bandwidths and large dispersive gains, which correspond to larger time bandwidth product waveforms, demonstrated more suitability for windowing (at energy levels less than 99.9%) in terms of sidelobe properties. The waveform autocorrelation function properties, such as resolution illustrated in Figure 4-10, were more sensitive to time windowing than cross-correlation performance. Using the effective symbol duration in the time domain, the desired energy level resulting from time windowing must be determined at the application level and guided by metrics of interest. The Brown symbol design process provides the flexibility to tailor symbol properties to meet specific requirements.

5.3.3 *Nonlinear Ambiguity Suppression (NLAS) Performance*

The newly developed VS piecewise-based Brown symbols were used with NLAS processing to demonstrate *M*-fold ambiguity suppression capability in a noisy channel. For the first ambiguous target scenario, two ambiguous signals having zero time delay were added to the desired unambiguous signal such that they *completely overlapped* in time. Despite the presence of two undesired ambiguous signal responses having +24.0 dB more signal power, relative to the weaker desired unambiguous signal, the NLAS processor effectively suppressed the ambiguous responses. The peak NLAS output response of the desired signal was approximately 11.0 dB above the noise floor (Figure 4-20) and the undesired ambiguous responses were suppressed an average of 10.0

to 13.0 dB (Table 4-6) – a net improvement of approximately 21.0 to 22.0 dB was realized. This performance was superior to equivalent Matched Filter (MF) processing (Figure 4-15) which was unable to detect the "buried" unambiguous signal. For the second ambiguous target scenario, the two ambiguous signals were time delayed such that they only *partially overlapped* the unambiguous signal (±50% in opposite directions). In this case, the unambiguous signal was discernable using conventional MF processing (Figure 4-16) primarily due to the superior compression and dispersion properties of the coded waveforms. As in the first scenario, the NLAS processing effectively suppressed all the ambiguous energy and induced minimal "coloration" on the unambiguous signal response (Figure 4-23). The "loss" of desirable unambiguous energy resulting from NLAS processing and the use of adaptive reserved code thresholding was less than 1.0 dB for all cases considered (Table 4-17).

The effectiveness of NLAS ambiguity suppression was also demonstrated for LFM coded waveforms and Brown symbols generated using sinusoidal and Constant Slope (CS) piecewise basis functions. For sinusoidal-based Brown symbols, both NLAS and MF processing were ineffective at detecting the unambiguous signal having coded symbol specifications of Table 4-10. Although the sinusoidal-based Brown waveforms are optimal from an rms time duration perspective, the VS piecewise-based symbols with lower PCCL levels provided superior signal detection. The CS piecewise-based Brown symbols, as implemented with sub-optimal dispersion, provided relatively equivalent signal detection and ambiguity suppression performance as the VS piecewise-based Brown symbols. Comparing NLAS processing using LFM coded waveforms with a

constant threshold, NLAS processing with piecewise-based Brown symbols and adaptive reserved code thresholding provides relatively equivalent performance in signal detection as indicated by the 11.0 dB difference in peak-to-noise floor responses shown in Table 4-16 and Table 4-18. The NLAS signal processing technique improved signal detection by an average of +8.5 dB compared to traditional matched filter processing.

5.4 *Significant Research Contributions*

This research has made significant progress in developing and employing near-optimum Brown symbols with NLAS processing to suppress range ambiguous responses. The knowledge base regarding the impact(s) of envelope exchange implementation for optimizing symbol PCCL performance is successfully expanded. The VS piecewise-based Brown symbols, developed and characterized under this research, provide equivalent NLAS signal detection performance as LFM coded waveforms. However, the $M = 2$ constraint of LFM coding is removed and Brown symbol demonstration paves the way for M-channel ($M > 2$) NLAS applications. Palermo's vision of achieving M-fold ambiguity suppression capability is now much closer to reality.

5.5 *Recommendations for Future Work*

The complexity of NLAS demonstrations must be increased using pulse diverse radar data containing the effects of clutter and complex target returns. NLAS ambiguity suppression capability using Brown symbols must be demonstrated in an environment containing realistic propagation factors and operational conditions. Such an effort would

truly show the potential enhancement that NLAS processing can provide systems requiring enhanced clutter suppression.

The application of Brown symbols beyond the NLAS framework must be investigated further. Some preliminary work on terrain-following radar applications suggest that Brown symbols may provide some improvement over current Walsh code implementations. The fine resolution offered by these waveforms promise great potential for radar applications such as terrain mapping. Other technology areas such as communications requiring multiple access capability and navigation aided precision location may benefit from mutually dispersive nature of the symbols.

BIBLIOGRAPHY

1. Cook, C.E and M. Bernfeld. *Radar Signals: An Introduction to Theory and Application.* Orlando: Academic Press, 1967.

2. Palermo, et al. "Ambiguity Suppression by Non-Linear Processing," *Record of the Eighth Annual Radar Symposium (June 1962)*

3. Brown, Wm.M. "Mutually Dispersive Codes for Nonlinear Suppression of Ambiguities." Draft AFRL/SN Paper, August 2001.

4. Barton, D.K. *Radars (Pulse Compression), Vol III.*. Dedham, MA: Artech House, Inc, 1975.

5. Skolnik, M.I. *Introduction to Radar System 3rd Ed.* New York: McGraw Hill, 2001.

6. Stremler, F.G. *Introduction to Communication Systems 3rd Ed.* New York: Addison-Wesley, 1990.

7 . Klauder, J.R. et al. "The Theory and Design of Chirp Radars," *The Bell System Technical Journal, vol. XXXIX(4):* 745-808 (July 1960)

8. Guey, J., and M. Bell, "Diversity Waveform Sets for Delay-Doppler Imaging," *IEEE Transactions on Information Theory, 44*(4): 1504-1522 (July 1998).

9 Rihaczek, A.W., *Principles of High-Resolution Radar*, New York: McGraw-Hill, 1969.

10. Gabor, D. "Theory of Communication," *J. Inst. Elec. Engrs. (London), pt. III, vol. 93*: 429-457 (1946).

11. Nathason, F.E. *Radar Design Principles*. Mendham, NJ: SciTech, 1999.

12. Lee, W.K and K. Park. "Optimal Sampling of Linear FM and Conversion to Digitized Waveform Having Predictable Sidelobe Patters", *IEEE 2001 CIS Conference* pp.(515-519)

13. Ramp, H.O. and E. Wingrove, "Principles of Pulse Compression," *IRE Transactions on Military Electronics*, *Vol 2*, 109-116 (April 1961)

14. Anderson, Jon M. *Nonlinear Suppression of Range Ambiguity in Pulse Doppler*. PhD dissertation, Air Force Institute of Technology (AETC), 2001 (ADA397364)

15. Lei, W., et al. "Resolution of Range and Velocity Ambiguity for a Medium Pulse Doppler Radar," *Record of the IEEE 2000 International Radar Conference, IEEE AESS*, 2000.

16 . Morris, G. and L. Harkness. *Airborne Pulsed Doppler Radar, 2nd Edition*. Artech House, 1996.

17. Anderson, J.M. et al. "Nonlinear Suppression of Range Ambiguities in Pulse-Diverse Radar," *IEE Electronic Letters*, Vol. 37, No. 20, September 2001, pp. 1251-1253.

18 Papaphotis, M.J. *An Analysis of Mutually Dispersive Brown Symbols for Non-Linear Ambiguity Suppression*. M.S. Thesis, Air Force Institute of Technology (AETC), 2002 (ADA401636).

19. Anderson, J.M. et al. "A Nonlinear Suppression Technique for Range Ambiguity Resolution in Pulse Doppler Radars," *Proceedings of the 2001 IEEE Radar Conference, Atlanta, Georgia*, May 2001, pp 141-146.

20. Brown, Wm.M. "Mutually Dispersive Codes for Nonlinear Suppression of Ambiguities." Draft AFRL/SN Paper, August 2001.

REPORT DOCUMENTATION PAGE

Form Approved
OMB No. 074-0188

1. REPORT DATE *(DD-MM-YYYY)*	2. REPORT TYPE	3. DATES COVERED *(From – To)*
25-03-2003	**Master's Thesis**	June 2002 – March 2003

4. TITLE AND SUBTITLE

DEVELOPMENT OF VARIABLE SLOPE PIECEWISE-BASED BROWN SYMBOLS FOR APPLICATION TO NONLINEAR AMBIGUITY SUPPRESSION

5a. CONTRACT NUMBER

5b. GRANT NUMBER

5c. PROGRAM ELEMENT NUMBER

6. AUTHOR(S)

Kurian, John, Captain, USAF

5d. PROJECT NUMBER

5e. TASK NUMBER

5f. WORK UNIT NUMBER

7. PERFORMING ORGANIZATION NAMES(S) AND ADDRESS(S)
Air Force Institute of Technology
Graduate School of Engineering and Management (AFIT/EN)
2950 Hobson Way
WPAFB OH 45433-7765

8. PERFORMING ORGANIZATION REPORT NUMBER

AFIT/GE/ENG/03-12

9. SPONSORING/MONITORING AGENCY NAME(S) AND ADDRESS(ES)
Attn: William M. Brown
AFRL/SN
WPAFB OH 45433-7765
DSN: 785-3627
william.brown@wpafb.af.mil

10. SPONSOR/MONITOR'S ACRONYM(S)
AFRL/SN

11. SPONSOR/MONITOR'S REPORT NUMBER(S)

12. DISTRIBUTION/AVAILABILITY STATEMENT
APPROVED FOR PUBLIC RELEASE; DISTRIBUTION UNLIMITED.

13. SUPPLEMENTARY NOTES
AFIT Technical POC: Michael A. Temple, AFIT/ENG
michael.temple@afit.edu

14. ABSTRACT

In 1962, Palermo used two conjugate Linear Frequency Modulated (LFM) pulses to demonstrate a Non-linear Ambiguity Suppression (NLAS) technique to reduce ambiguous energy in radar returns. Using conjugate LFM pulse coding does not readily extend to larger symbol families and thus is severely limited for *M*-channel ($M > 2$) NLAS applications. Larger families of optimal mutually dispersive codes with higher time bandwidth products are needed to achieve the desired *M*-fold range ambiguity reduction.

Using correlation function rms time duration as an optimization metric, the recently proposed Brown's theorem formulates a deterministic process for designing optimal mutually dispersive symbol sets of arbitrary size. The rms time duration perfor-mance of digitized "Brown" symbols is invariant to choice of basis (phase-rate) functions used in the design process, yet improvement in cross-correlation sidelobe performance is directly linked to basis function design. This insight provided the impetus for designing and synthesizing a new set of mutually dispersive symbols based on Variable Slope (VS) piecewise basis functions. The resultant VS piecewise-based "Brown" symbols are used with NLAS processing to demonstrate *M*-fold ambiguity suppression capability. Despite the presence of two undesired ambiguous signal responses having +24.0 dB more signal power relative to the weaker desired unambiguous signal, the NLAS processor effectively suppressed the ambiguous responses. The desired signal peak NLAS output response was approximately 11.0 dB above the noise floor and undesired ambiguous responses were suppressed an average of 10.0 to 12.0 dB – a net improvement of approximately 21.0 to 22.0 dB

15. SUBJECT TERMS

Ambiguity Suppression, Diverse Pulse Coding, Brown Symbols

16. SECURITY CLASSIFICATION OF:			17. LIMITATION OF ABSTRACT	18. NUMBER OF PAGES	19a. NAME OF RESPONSIBLE PERSON
a. REPORT	b. ABSTRACT	c. THIS PAGE			Dr. Michael A. Temple, AFIT/ENG
U	U	U	UU	96	19b. TELEPHONE NUMBER *(Include area code)* (937) 255-3636, ext 4703